EXPERIMENTAL INVESTIGATION OF FRACTURE OF GRANITE UNDER COMPRESSION

Robert Grabenian
John D. O'Keefe
Kenneth K. Overoye

FINAL REPORT

15 December 1971

Sponsored by
Advanced Research Projects Agency
ARPA Order No. 1779, Amendment 2
Program Code No. 1F10

The views and conclusions contained in this document are those of the authors and should not be interpreted as necessarily representing the official policies, either expressed or implied of the Advanced Research Projects Agency or the U.S. Government.

Prepared by
Advanced Technology Staff Group
Space Vehicles Division
TRW SYSTEMS GROUP
One Space Park
Redondo Beach, California

R-79

Unclassified
Security Classification

DOCUMENT CONTROL DATA - R & D

(Security classification of title, body of abstract and indexing annotation must be entered when the overall report is classified)

1. ORIGINATING ACTIVITY *(Corporate author)*
TRW Systems Group
One Space Park
Redondo Beach, California 90278

2a. REPORT SECURITY CLASSIFICATION
Unclassified

2b. GROUP

3. REPORT TITLE
Experimental Investigation of Fracture of Granite Under Compression

4. DESCRIPTIVE NOTES *(Type of report and inclusive dates)*
Final Report, 10 March 1971 - 20 December 1971.

5. AUTHOR(S) *(First name, middle initial, last name)*
Robert Aprahamian
John D. O'Keefe
Kenneth R. Overoye

6. REPORT DATE
15 December 1971

7a. TOTAL NO. OF PAGES
78 79

7b. NO. OF REFS
4

8a. CONTRACT OR GRANT NO.
H0210040

b. PROJECT NO.
ARPA Order No. 1579, Amend. 2

c. Program Code No. 1F10

d.

9a. ORIGINATOR'S REPORT NUMBER(S)

9b. OTHER REPORT NO(S) *(Any other numbers that may be assigned this report)*

10. DISTRIBUTION STATEMENT
Distribution of this document is unlimited.

11. SUPPLEMENTARY NOTES

12. SPONSORING MILITARY ACTIVITY
Advanced Research Projects Agency

13. ABSTRACT

The applicability of laser holographic interferometry to study the deformations of geologic materials under applied stresses was investigated. Two types of geologic materials were studied - Jaspar Quartzite and Charcoal Granite. Two holographic interferometry techniques were employed. Double exposure holographic interferometry was used to study and record the deflections of the specimens from 0 psi to near-fracture. Data from the double exposure holograms provided radial and axial displacements along the length of the specimens. A computer program was utilized to deduce the radial and axial strains from the holographic data. Stored beam holographic interferometry was used together with high speed motion picture photography to record the deflections of the specimens from near-fracture to fracture.

DD FORM 1 NOV 65 1473

Unclassified
Security Classification

14. KEY WORDS	LINK A		LINK B		LINK C	
	ROLE	WT	ROLE	WT	ROLE	WT
Holography						
Holographic interferometry						
Rock mechanics						
Charcoal granite						
Jaspar quartzite						
Fracture mechanics						

EXPERIMENTAL INVESTIGATION OF FRACTURE OF GRANITE UNDER COMPRESSION

Robert Aprahamian
John D. O'Keefe
Kenneth R. Overoye

FINAL REPORT

15 December 1971

Sponsored by

Advanced Research Projects Agency
ARPA Order No. 1579, Amendment 2
Program Code No. 1F10

The views and conclusions contained in this document are those of the authors and should not be interpreted as necessarily representing the official policies, either expressed or implied of the Advanced Research Projects Agency or the U.S. Government.

Prepared by

Advanced Technology Staff Group
Space Vehicles Division
TRW SYSTEMS GROUP
One Space Park
Redondo Beach, California

FOREWORD

The work described in this report was performed by the Advanced Technology Staff Group of the Space Vehicles Division, TRW Systems Group, Redondo Beach, California. The Advanced Technology Group is under the direction of Dr. P. G. Bhuta. The work was sponsored by the Advanced Research Projects Agency (ARPA Order No. 1579, Amendment 2). It was performed under U.S. Department of Interior, Bureau of Mines, Contract No. H0210040. Mr. Clifford W. Schultz, Twin Cities Mining Research Center, Twin Cities, Minnesota served as Project Officer under this contract.

Project Manager at TRW Systems Group was Mr. R. Arrahamian with analytical support provided by Mr. J. D. O'Keefe and Dr. D. A. Evensen. Experimental support was provided by Messrs. K. R. Overoye and J. E. Wright. The authors wish to thank Mr. C. W. Schultz for supplying specimens and related data during the course of this investigation.

ABSTRACT

The applicability of laser holographic interferometry to study the deformations of geologic materials under applied stresses was investigated. Two types of geologic materials were studied - Jaspar Quartzite and Charcoal Granite. Two holographic interferometry techniques were employed. Double exposure holographic interferometry was used to study and record the deflections of the specimens from 0 psi to near-fracture. Data from the double exposure holograms provided radial and axial displacements along the length of the specimens. A computer program was utilized to deduce the radial and axial strains from the holographic data. Stored beam holographic interferometry was used together with high speed motion picture photography to record the deflections of the specimens from near-fracture to fracture.

TABLE OF CONTENTS

1.0 INTRODUCTION AND SUMMARY

This final report documents the results of the work performed by TRW Systems under Bureau of Mines Contract No. H0210040. The objective of the program was to demonstrate the feasibility of using holographic interferometry to study fracture in geologic materials. Fracture tests were performed on small cylindrical specimens. Ten specimens each of charcoal granite and Jaspar quartzite were supplied by the Bureau of Mines for use on this program. A loading fixture was fabricated to uniaxially compress these test cylinders.

Two holographic techniques were employed to measure the response of the specimens, namely, double exposure interferometry and stored-beam interferometry. Double exposure holographic interferometry was successfully used to study the incremental deflections of the specimens under increments in the axial load. It was found necessary to incrementally load the specimens so that the fringe densities would not be too large to resolve. By summing the incremental deflection obtained from each hologram, the total deflection of the specimens was determined. The interference fringe data contained on the holograms were reduced using a computer program to calculate axial and radial displacements and strains. These displacements and strains were calculated at all points along an axial line on the surface of the cylindrical specimens. However, the holographic technique and data reduction method is not restricted to a line and can be used to obtain data in all surface domains. The fringe patterns induced in Jaspar quartzite were smooth indicating that the displacement field was locally smooth. Therefore, on a local

level the rods were responding homogeneously. During the loading process there appeared global aberrations in the fringe patterns, these aberrations were interpreted as surface manifestations of fracturing, and revealed the points where fracturing was being initiated.

The fringe patterns induced in charcoal granite were not smooth indicating that the local displacement fields were inhomogeneous. This inhomogeneity would be expected because of the relatively large grains in these specimens. These local inhomogeneities were for the first time quantified, thus demonstrating an attribute of the holographic process - the extreme sensitivity. Also as before, global aberrations in the fringe patterns were related to regions of failure in the material.

Stored-beam holographic interferometry was used to study the response of the specimens to an applied load near their fracture stress level. A high-speed motion picture camera placed behind the stored-beam hologram recorded the fringes in real-time as the applied load was increased to cause failure. A study of the fringe motion, as obtained by a frame-by-frame analysis of the motion picture, provided some qualitative information regarding the fracture process. However, because of motion due to creep and other extraneous phenomena which occurred in the specimen between the time the hologram was exposed, developed and reinserted into its holder, the contribution to the fringe pattern by the motion due to the applied load was obscured.

Holographic double exposure interferometry process was shown to be a viable technique to study materials such as rocks which may exhibit a high degree of inhomogeneity and anisotropy. The drawback to the technique is that many exposures need to be obtained when the total

displacement to be measured is large. For the specimens tested, the number of holographic interferograms ranged from 15 to 25. This problem can be circumvented to a degree by desensitizing the interferometry process. The sensitivity can be decreased by approximately an order of magnitude by various viewing and illumination configurations. In the tests, the absolute fringe order was not known unambiguously. By using finite fringe interferometry and possibly simultaneously double exposure interferometry, the absolute order can be determined. The implementation of the above techniques, however, was out of scope of the present effort but is recommended for future work.

Unfortunately, the problems associated with stored-beam holographic interferometry to study fracture in geologic materials are much greater than with double exposure interferometry techniques. The principal difficulty is due to extraneous motion of the rock specimens (i.e., creep) which contributes to the fringe pattern. There is currently no known method which can be used to overcome this difficulty. Perhaps by using photochromics or thermoplastics (which do not require the photographic developing process) to eliminate the use of film, the time between making the hologram and performing the test can be sufficiently shortened to overcome this problem. Such development was beyond the scope of this program.

Additional work in geologic testing is needed to study the applicability of holographic techniques to dynamic fracture conditions, i.e., the study of fracture growth. Since fracture growth is a highly dynamic event, such tests would require the use of pulsed-ruby holography.

In pulsed-ruby holography laser pulses as short as 3 nanoseconds in duration are used to freeze the motion of high-speed dynamic events. Pulsed-laser holography has been used at TRW to study wave propagation in rods, beams, plates, and shells. The technique appears equally promising for studying dynamic fracture.

2.0 EXPERIMENT DESCRIPTION

2.1 Granite Specimens

Twenty geologic specimens -- ten Jaspar Quartzite and ten Charcoal Granite -- were supplied to TRW by the U.S. Bureau of Mines, Twin Cities, Minnesota. The specimens were ground and polished right circular cylinders measuring one inch in diameter by two inches long. Figure 1 shows a photograph taken of one of the Charcoal Granite specimens. Technical data concerning the specimens were also supplied by the Bureau of Mines. The data pertinent to this program is summarized in Table I.

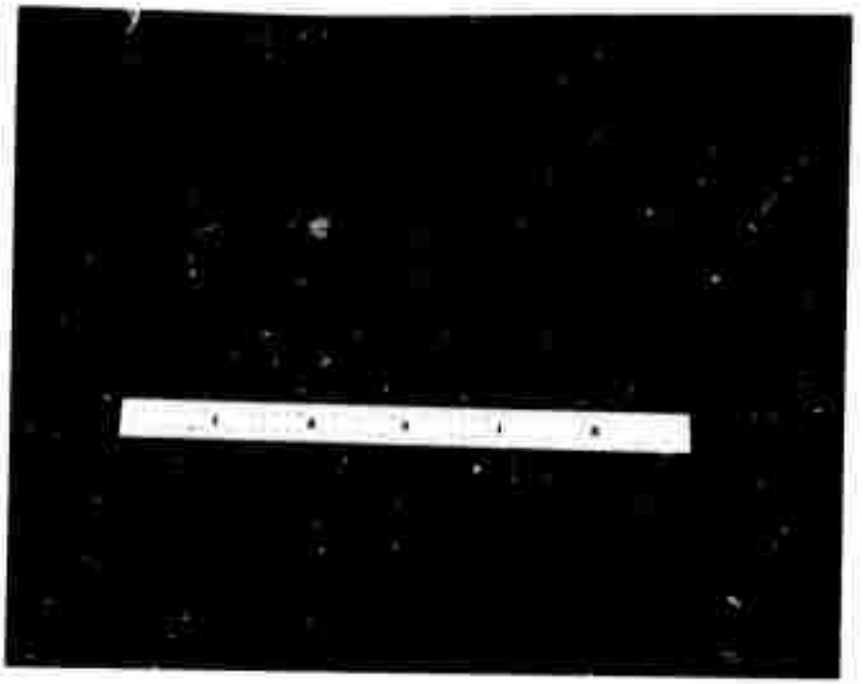

Figure 1: Photograph showing one of the specimens (Charcoal Granite) used in this investigation

TABLE I

Compressive strength, Young's Modulus and Poisson's Ratio for the Jasper Quartzite and Charcoal Granite Specimens used in this Investigation (supplied by the U.S. Bureau of Mines.*)

Specimen Type	Jasper Quartzite	Charcoal Granite
Compressive Strength (PSI)	$59.74 \cdot 10^3$	$39.11 \cdot 10^3$
Standard deviation	$5.01 \cdot 10^3$	$1.72 \cdot 10^3$
Coefficient of variation (percent)	8.4	4.4
Young's Modulus (PSI)	$7.749 \cdot 10^6$	$7.748 \cdot 10^6$
Standard deviation	$.334 \cdot 10^6$	$.300 \cdot 10^6$
Coefficient of variation (percent)	4.3	3.8
Poisson's Ratio	.1332	.2479
Standard deviation	.0096	.0044
Coefficient of variation (percent)	7.2	1.8

2.2 Loading Mechanism

A loading fixture was specially designed and fabricated for use on this program. The fixture was designed to meet two criteria. One criterion was that the fixture be sufficiently small that it could be placed on a stable, granite table used in holography. Continuous wave

* Data taken from memorandum to David A. Larson, Engineering Technician Twin Cities Mining Research Center, from Peter G. Chamberlain, Geophysicist, Twin Cities Mining Research Center, Twin Cities, Minnesota, May 28, 1970.

holography was used with all experiments, requiring that all components be placed on a stable working surface. The other criterion was that a clear view to the specimen be provided. Holography being an optical technique requires an unobstructed line of sight from the hologram to the object under investigation. The loading fixture is shown in Figure 2. Referring to Figure 2, the specimens are compressed axially between a lower anvil and an upper pressure bar. The anvil rested on a two inch thick steel plate.

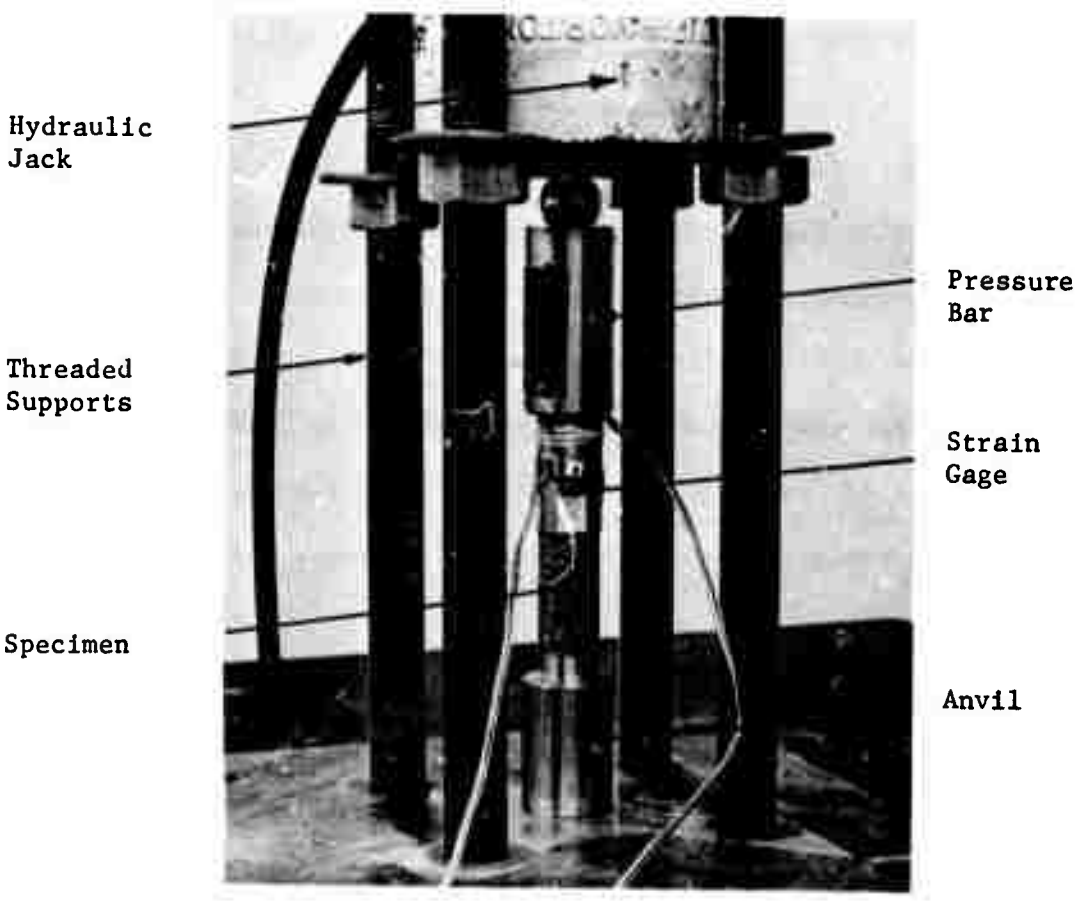

Figure 2: Photograph of the loading mechanism constructed for the tests

Both the anvil and the pressure bar were made from type 303 stainless steel. No lubrication or any other device was used between the steel and specimen interface to control the boundary condition. A compressive force was applied to the pressure bar by the expansion of a hydraulic jack causing tension in the four threaded support rods. The hydraulic jack was actuated by a small hydraulic hand pump capable of delivering over 5000 psi of fluid pressure to the jack. The area of the piston in the jack was approximately 10 square inches; hence, over 50,000 pounds total force could be developed in the system. This load, if applied to the one inch diameter specimen, would result in applied stresses exceeding 65,000 psi.

Four calibrated strain gages were installed at 90 degree intervals around the steel pressure bar, just above the face of the sample. The output from these gages were monitored to assess the degree of uniformity of the applied stresses. By adjusting the relative lengths of the threaded support rods, uniformity of the applied stress could be maintained to ± 10 percent. The spherical steel ball between the jack face and the pressure bar also aided in achieving a uniformly applied stress.

The pressure of the hydraulic fluid was measured with a mechanical pressure gage. The precise area of the jack piston was 11.03 square inches. Hence the force, F, developed by the jack with a hydraulic pressure, p, was $F=11.03\ p$. The stress then applied to the specimen was $P=F/A$, where $A = \frac{\pi}{4}(1.0)^2$ is the area (in square inches) of the specimen faces. The relationship between the applied stress, P, and the hydraulic pressure, p, is given by

$$P = \frac{11.03}{(\pi/4)\ (1.0)}\ p$$

or

$$P = 14.05\ p$$

2.3 Holography Set Up

2.3.1 Holography

The term "holography" is used to describe a means of recording the amplitudes and phases of waves, such as light or sound. Holography originated with Gabor (1) who pointed out the possibility of recording on a photographic plate the amplitudes and phases of coherent, monochromatic light waves transmitted through a transparent object. By projecting light through the developed photographic plate (i.e., the "hologram") a three-dimensional virtual image of the original object is reconstructed.

The reproduction of images as Gabor suggested became practical with the advent of the laser as a source of monochromatic, coherent light. In 1964, Leith and Upatnieks (2) demonstrated that a three-dimensional image of an opaque object could be reconstructed using an off-axis technique. Figure 3 shows a typical set-up of the apparatus used in the Leith and Upatnieks holographic method.

In making the hologram, light waves reflecting from an object (object beam) interact with undisturbed light as reflected by a mirror (reference beam). When the light forming the reference beam is in phase with the light forming the object beam the waves add; conversely, the waves cancel one another when they are out of phase. This type of interaction results in spatial variations in the intensity of the light striking the photographic film. Since photographic film reacts to the intensity of light impinging on it, the exposed film gives a permanent

record of the interaction of the two light beams. The variations are spatially minute and may be considered to form a fine, irregular diffraction grating on the photographic plate.

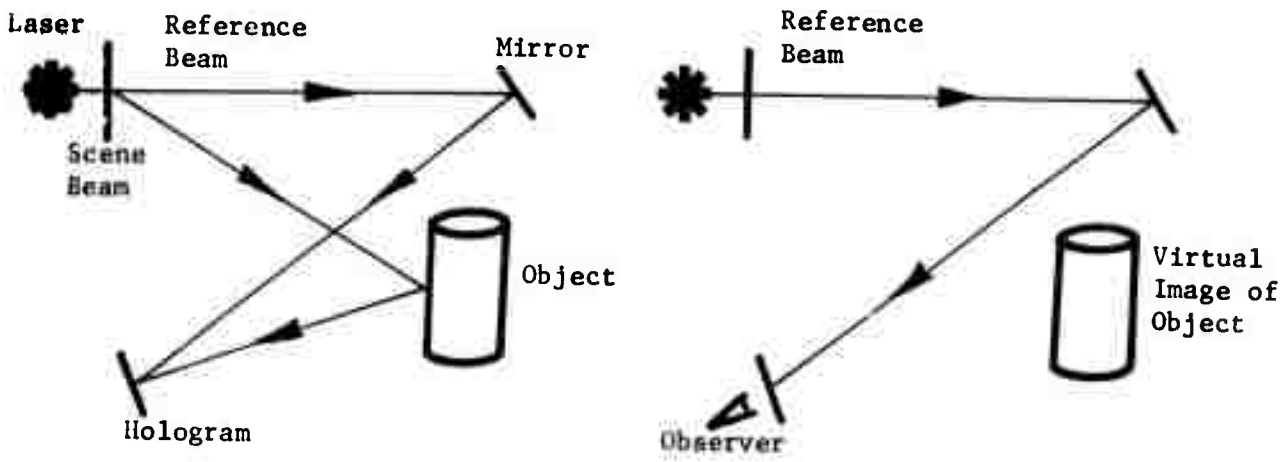

Figure 3: Left: Image Recording Process
Right: Image Retrieval

To reconstruct the image of the object from the hologram, the developed photographic film (or hologram) is illuminated with any monochromatic light source, for example, the original laser. The interaction of the light with the hologram results in the reconstruction of a three-dimensional image of the original object. It should be recognized from the description given above that entire surfaces (rather than isolated points) are recorded. It is also important to note that the object need no special surface preparation. Indeed, diffuse objects such as geologic specimens are more amenable to holography than are shiny, specular surfaces.

2.3.2 Holographic Interferometry

Although image reconstruction was the first application of holography, a technique that has more potential from an engineering

standpoint is "Holographic Interferometry". Two forms of holographic interferometry were used in this investigation, viz double exposure and stored beam. The essential ideas of double exposure holographic interferometry are as follows: first a hologram is made of the object under investigation; then the object is subjected to loads which cause it to deform, and the same hologram is exposed for a second time. When this "double-exposed hologram" is developed and illuminated, two images are reconstructed: one is of the undeformed body, the other of the deformed body. The coherent light waves which form the two reconstructed images interact with one another, thereby creating interference fringes over the image. By analyzing the fringe patterns, one can quantitatively determine the surface deformations of the body as a result of the applied load. Aleksandrov and Bonch-Bruevich (3) give expressions which relate the interference fringes to the surface deformation of the subject. Double exposure interferometry provides a permanent recording or interferogram of the stressed object for detailed evaluation after processing. Stored-beam holographic interferometry, on the other hand, provides the experimenter with a visual means of measuring deflection in real-time. This type of holography gives rise to "live" interference fringes, which shift and change as load is applied to the object. In the live fringe method, a hologram of the undeformed, stationary object is made and developed. This hologram is then very carefully put back in its original position, i.e., in the photographic plate holder where it was originally exposed. The hologram is then illuminated by the laser and the reconstructed image (viewed through the hologram) of the undeformed object is superimposed on the real object. Now suppose the object being studied

is allowed to deform; then the light from the deformed body (real object) interacts with the stored image of the undeformed body (produced by the hologram) and an interference fringe pattern is formed in real-time. This fringe pattern may be analyzed directly or photographed through the hologram. A motion picture camera may be used to record dynamically the shifts in the fringes due to a time varying load.

2.3.3 Relation of Holographic Fringes to Deformations of the Object

For the present program the interpretation of the fringe patterns obtained from the holograms is accomplished using the technique described by Aleksandrov and Bronch-Bruevich (3). The technique applies equally to either double exposure or stored beam techniques. It can be shown (3) that the dark fringes covering a body under stress are located wherever the condition

$$\vec{\delta} \cdot (\hat{s} + \hat{c}) = \frac{(2n-1)}{2} \lambda \qquad (1)$$

is satisfied; where

$\vec{\delta}$ = displacement vector representing the deformation of the object at a point on its surface

λ = wavelength of the light from the laser used to make and reconstruct the holographic images

$\hat{c}$ = unit vector in the direction from the object to the illuminating source

$\hat{s}$ = unit vector in the direction from the object through the hologram to the observer

n = integer, ± 1, ± 2, ± 3, ...

The term $\vec{\delta} \cdot (\hat{s} + \hat{c})$ is best understood using the vector diagram depicted in Figure 4.

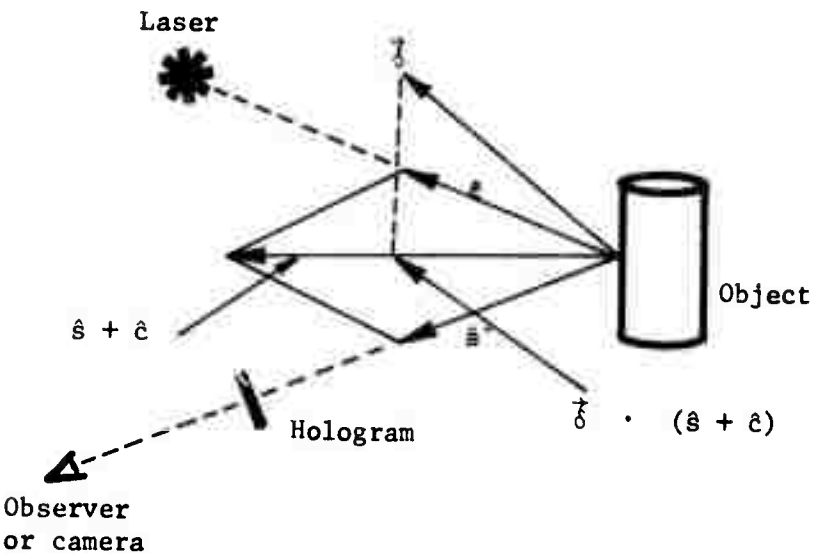

Figure 4: Vector diagram showing the relationships between the vectors used in Eq. 1.

The term $(\hat{s} + \hat{c})$ represents a vector bisecting the angle between vectors $\hat{c}$ and $\hat{s}$ having a length 2 cos 1/2 $(\hat{s}, \hat{c})$. Hence the term $\vec{\delta} \cdot (\hat{s} + \hat{c})$ represents the component of deflection, $\delta_{c,s}$ in the direction of a unit vector bisecting the angle between the viewing and illuminating direction times a factor 2 cos 1/2 $(\hat{s}, \hat{c})$. Hence, Equation 1 can be written

$$\delta_{c,s} = \frac{(2n-1)\lambda}{4 \cos 1/2\ (\hat{s}, \hat{c})} \qquad (2)$$

Qualitatively, the fringes seen over the object represent lines of constant displacement in the direction of the vector $\hat{e} + \hat{s}$. If parallel light is used to illuminate the object and the angle subtended by the object from the position of the observer is less than 1°, then the vector $\hat{e} + \hat{s}$ can be considered constant for all points on the object surface.

2.3.4 Evolution of the Holography Set Up

The discussion of the preceding section showed that for a single choice of illumination and observation directions, $\hat{e}$ and $\hat{s}$, respectively, holographic interferometry measures only the component of deformation along a line bisecting the directions $\hat{s}$ and $\hat{e}$. It is obvious, therefore, that if the measurement of more than one components of the deformation is desired, then data using more than one observation and/or illumination direction is required. Although it is not practical to illuminate an object from more than one direction, it is a straight forward matter to observe a given point from two or more directions. One may either view the point in question from two or more vantage points behind a single hologram, or from two or more widely separated holograms. In the interest of greater precision, the latter approach was selected.

The number and location of the holograms, and of the illuminating direction, were governed to a large extent by the geometrical properties of the specimens and the loading conditions. Since the specimens were cylindrically symmetric and they were compressed uniaxially, the deformations over their surfaces were expected to be axisymmetric. Therefore, a plane of symmetry was established passing through the axis of the specimens. Figure 5 is a conceptual diagram showing the specimens and the plane. Where this plane intersects the specimen surface, the deformation vectors all were expected to lie in the plane. Along the line of

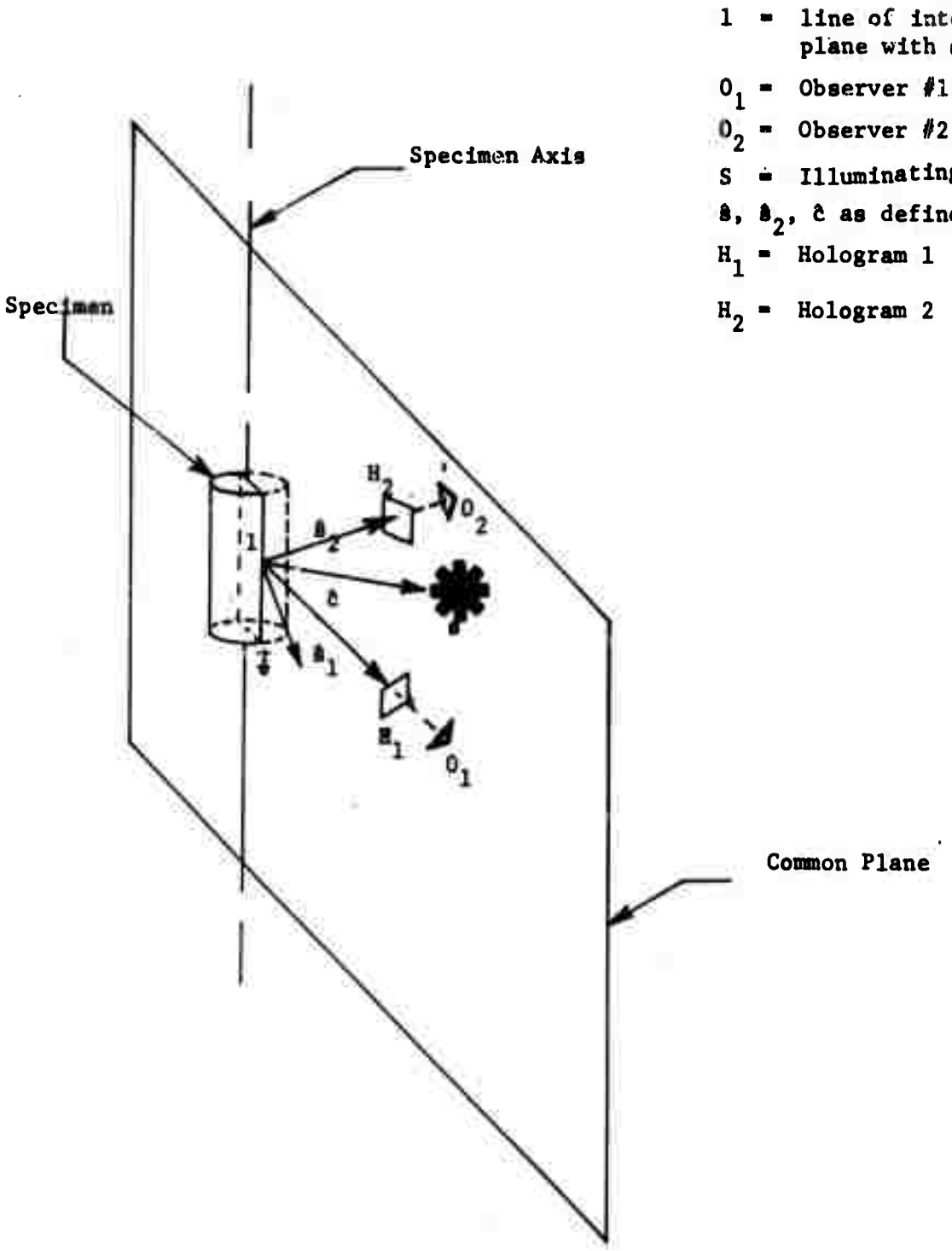

Figure 5: Conceptual diagram showing two observers, the illuminating source and the specimen axis lying in a common plane

intersection of the reference plane with the surface, only radial and axial components of the deformations would have to be determined. To measure these components holographically, the illumination vector was made to lie in the reference plane and two holograms were positioned so that two observation vectors would also lie in the plane.

Poisson's ratio for the materials were .13 and .25 (Table I). Consequently, the radial deformations were expected to be much smaller than the axial displacements. Therefore, it was desirable that for one of the observation stations, (0_1 or 0_2), the component measured, δ_{cs}, would be the radial component alone. The other station would measure a combined axial and radial displacement, from which the radial component could be subtracted (a small correction) to give the axial displacement.

One further step was required before the final system was designed. For an observer (0_1 or 0_2) located a reasonable distance from the specimens, the observation vector changes a small, but significant, amount for different points on the specimen. If the illuminating beam were collimated, then the illumination vector, $\hat{e}$, would remain constant for various points on the cylinder. Consequently, the bisector, and hence δ_{cs}, would not be directed in the same direction for various points over the objects. Measurement of this radial component alone by one of the observers would not be possible. It was found, however, that if a converging illuminating beam were used, then pure radial deflection alone could be measured by one of the observers <u>for all points</u> along the line, 1, of intersection of the reference plane with the specimen (cf., Figure 5).

The compensating effects of a converging illumination beam may be described with the aid of Figure 6. For three points on the object, observation vectors, $\hat{s}$, and illumination vectors, $\hat{c}$, are shown. The bisectors, $\hat{s} + \hat{c}$, at each point can be seen to be parallel. The components of the deformation, measured, $\delta_{c,s}$, are parallel to the bisectors. The components measured, therefore, are all in the same direction over the height of the object. The compensation is exact over a plane halfway along, and normal to, the line joining the virtual source and the observer. The departures from precise compensation for points near, but not on the plane, remain negligible.

To summarize, a holographic set up evolved for which (1) a single illumination source and two observer positions would be used; (2) the source, observers and specimen axis would all lie in a common plane; and (3) a converging illuminating beam would be used, the focal point of which was equal in distance from the specimen axis as from the axis to one of the observers. Bringing these three criteria together, Figure 7 shows a scale drawing of the relative locations of the specimen, observer locations 1 and 2, and the focus of the converging illuminating beam. For practical data reduction, the observers were replaced by cameras with their lens entrance aperatures at the locations shown. For double exposure interferograms of the specimens under stress, a still camera was used to photograph the image and fringe patterns. For stored beam interferograms, a high speed motion picture camera was used to record the resulting changes in the fringe patterns as the specimens were compressed.

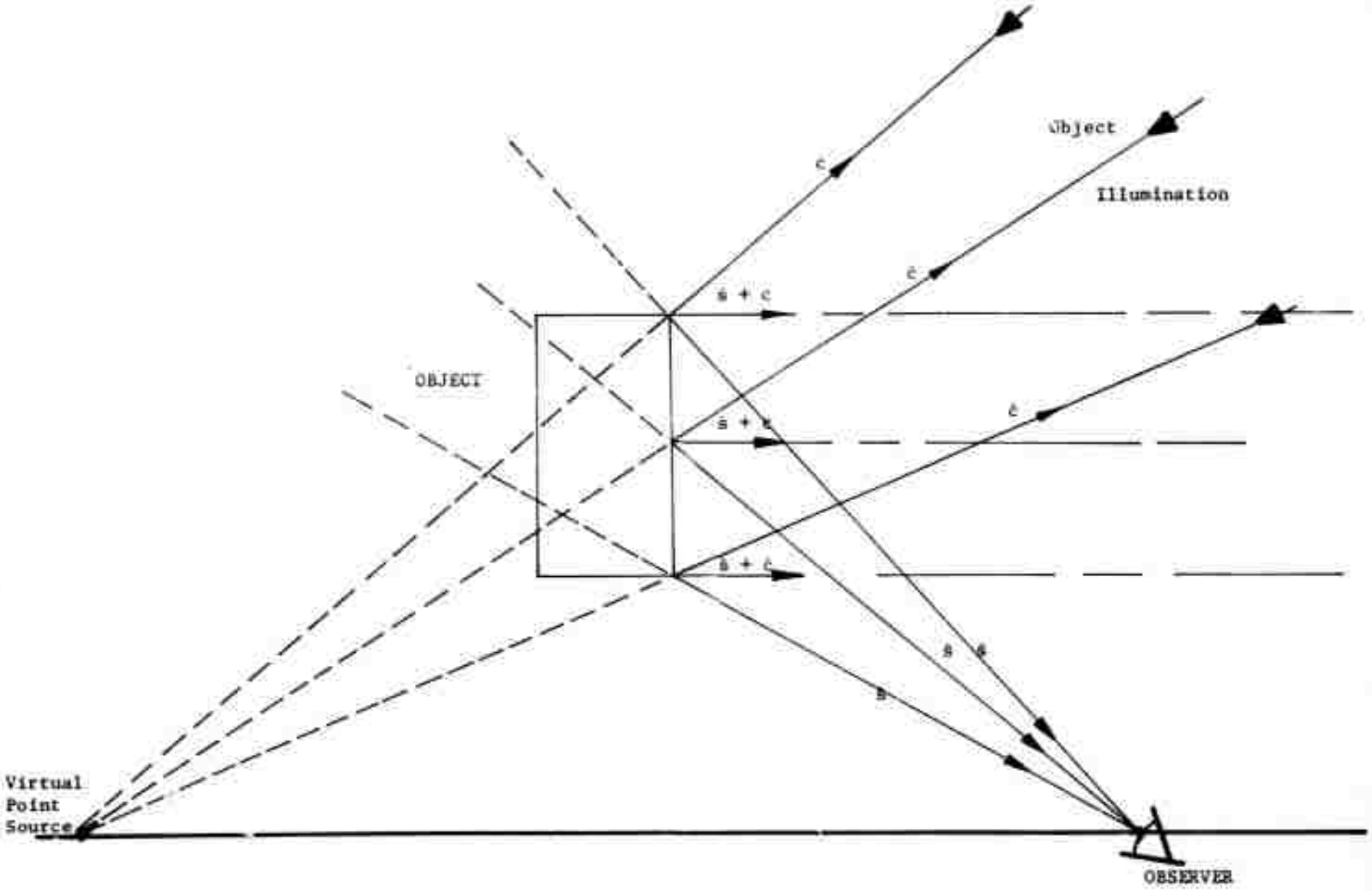

Figure 6: Diagram showing how the direction of $(\hat{s} + \hat{c})$ and hence the direction of $\delta_{c,s}$, remains constant over the height of the object when a converging illuminating beam is used.

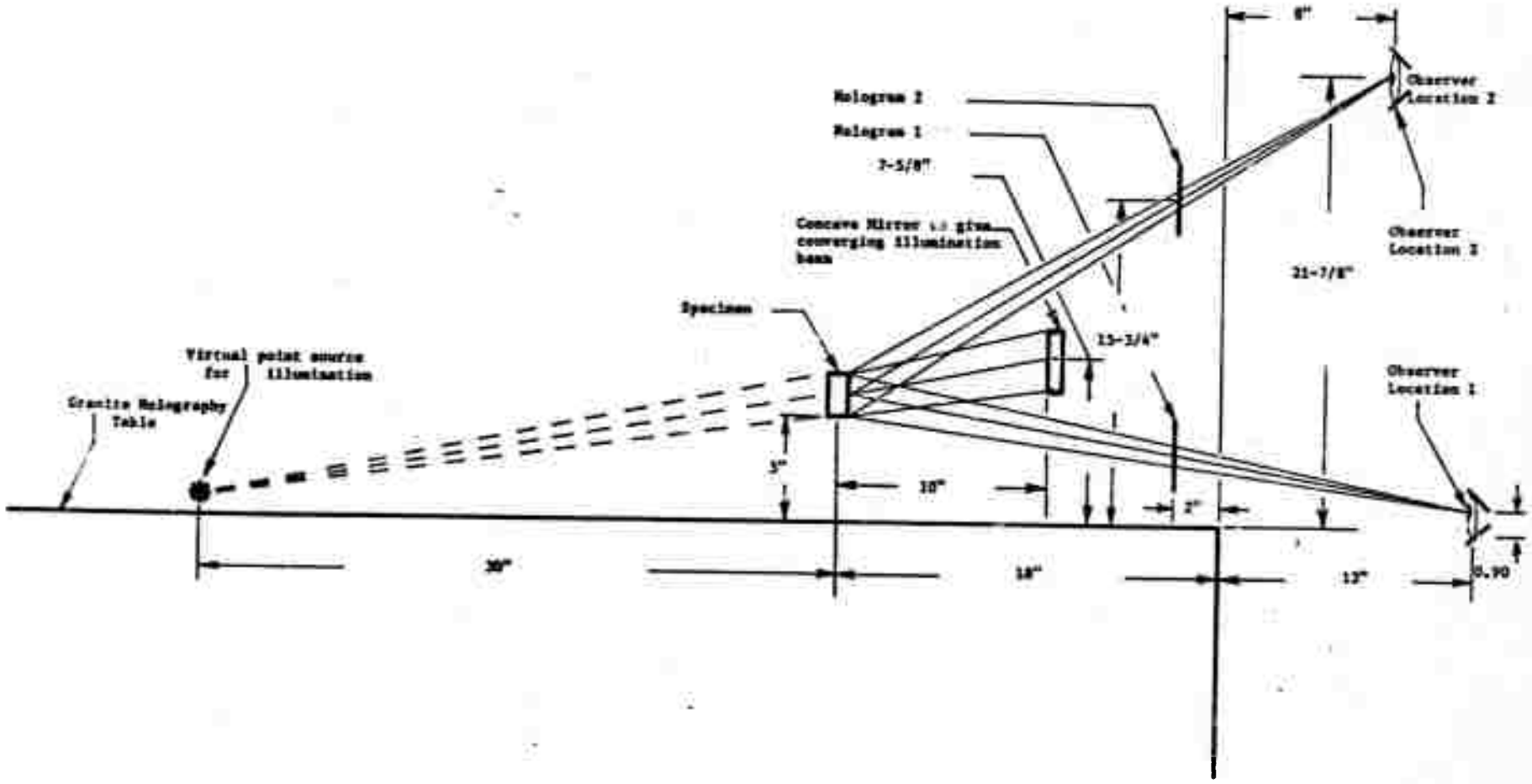

Figure 7: Scale drawing of relative postions of the specimen, holograms, observer locations and virtual illumination source

Figure 8 is a photograph showing a specimen in place in the loading fixture. The relative positions of the two holograms can be seen. The large mirrors to the right side were used to direct the reference beams to the hologram plates. Figure 9 is a diagram of the overall holography set up, showing the laser source and paths of the specimen illuminating beam and the two reference beams (required for the holograms). Figure 10 shows a photograph taken of the overall set up. The laser used for the initial tests was a 15 milliwatt Helium Neon continuous wave (cw) laser. The laser used for the final tests and motion picture holography was a cw Argon ion laser emitting 300 milliwatts at a wavelength of 5145Å.

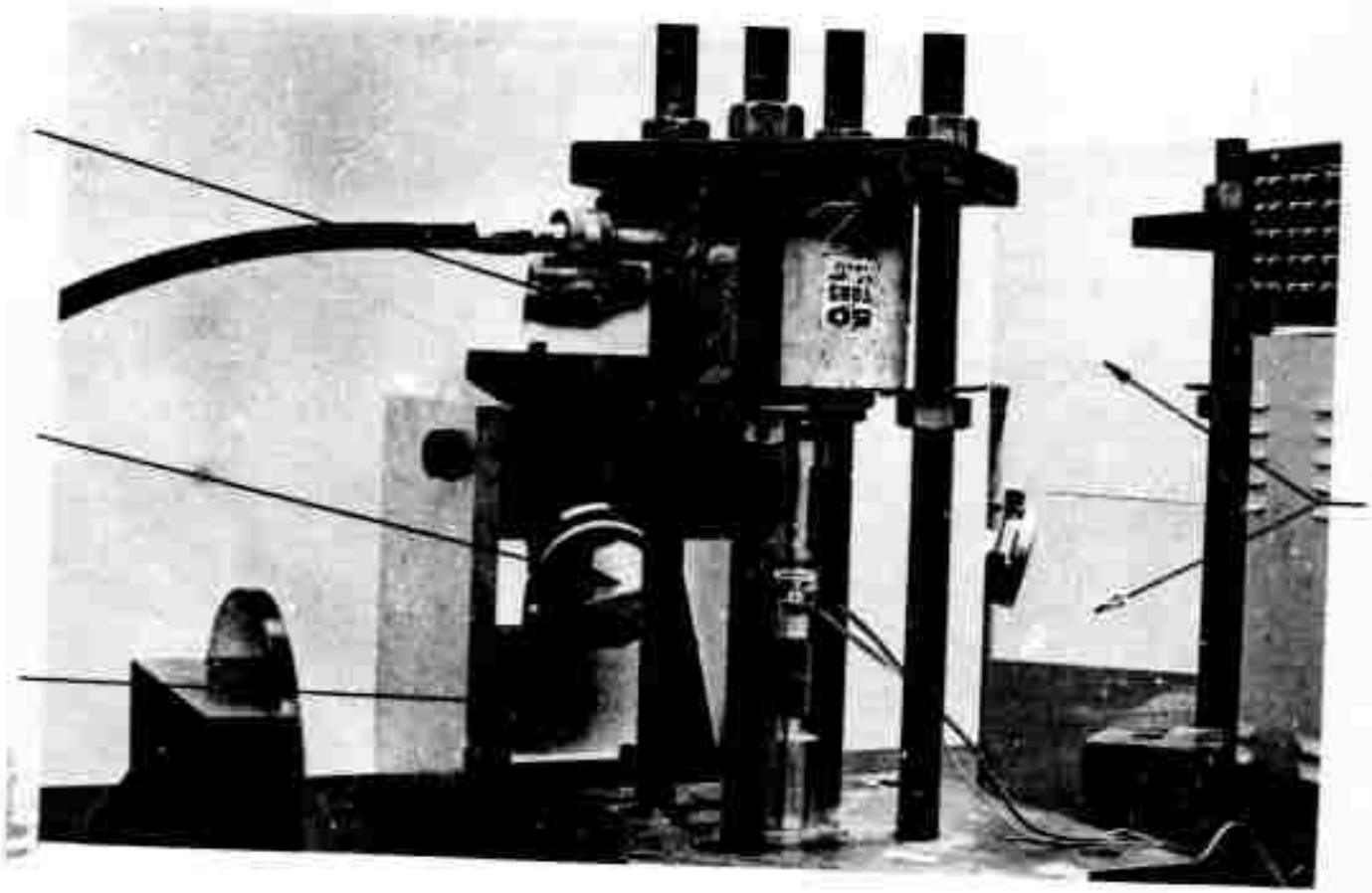

Figure 8: Photograph showing the specimen in the loading aparatus and the two glass hologram plates in the background

BS = Beam Splitter

CL = Collimating Lens

CM = Concave Mirror

H = Holograms (1 & 2)

SF = Spatial Filter

VBS = Adjustable Beam Splitter

VPS = Virtual Point Source

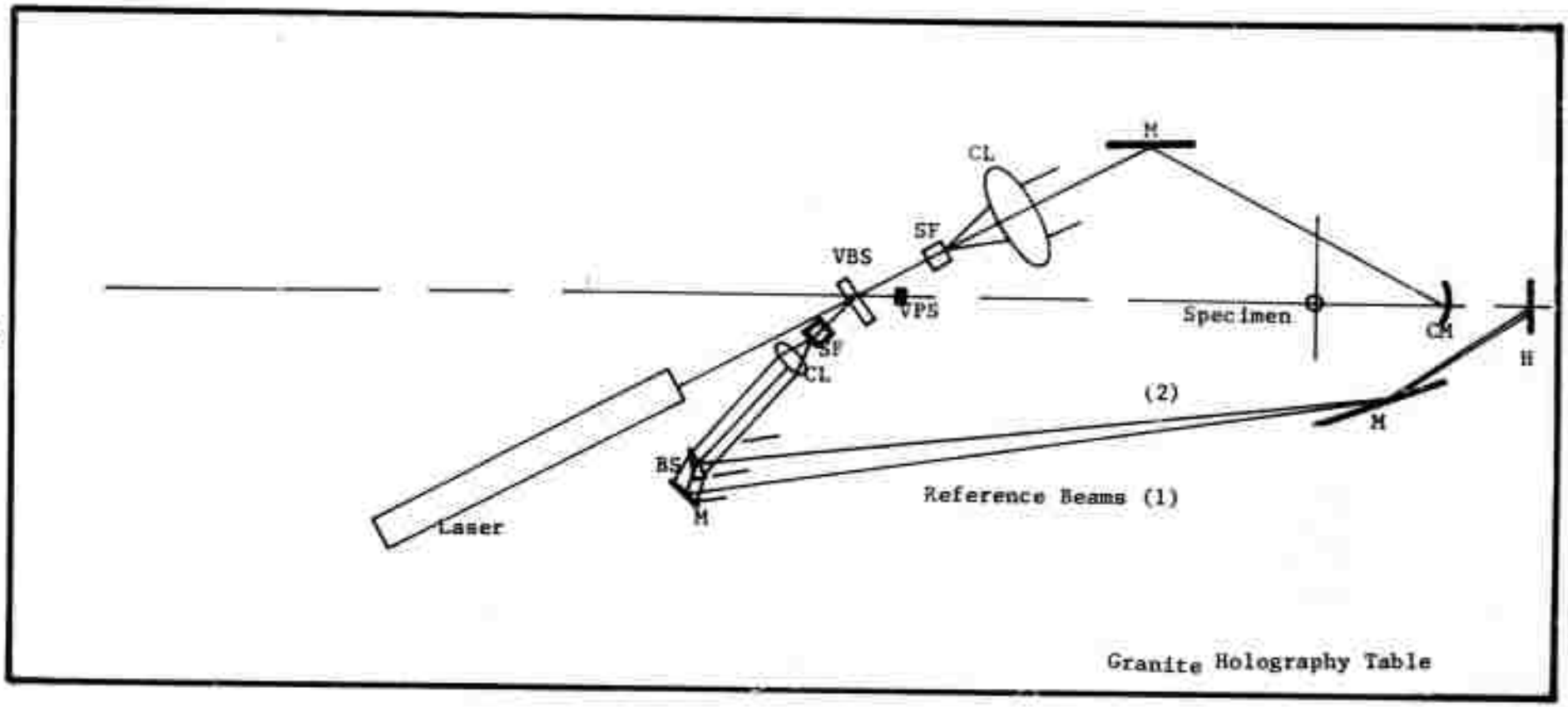

Figure 9: Diagram of the overall holography set up

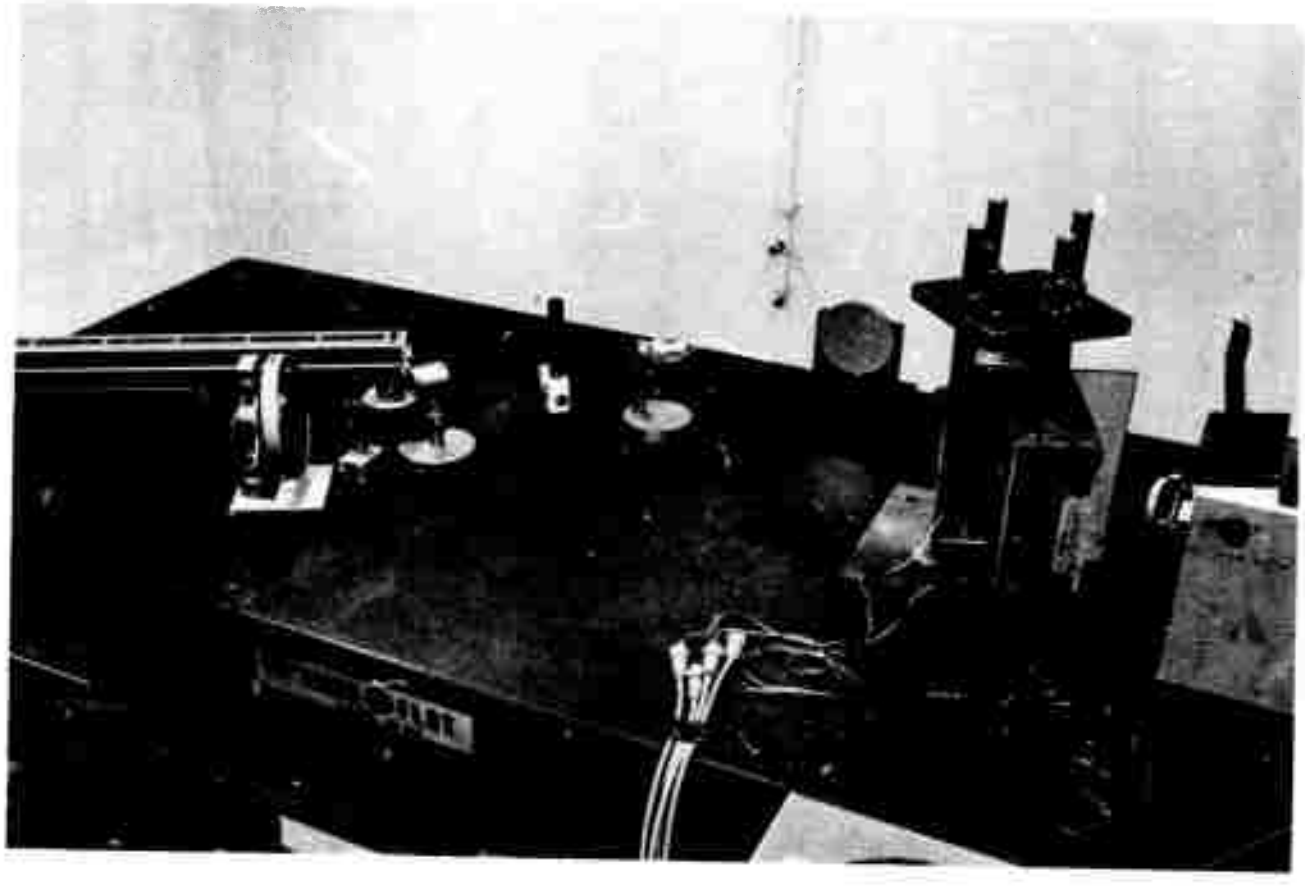

Figure 10: Phctograph of the overall test setup

3.0 EXPERIMENTAL PROCEDURE

3.1 Double Exposure Holography

A few of each type of the geologic specimens were crushed in preliminary tests to check out the loading fixture and to establish approximate failure levels so that an appropriate procedure to record double exposure holograms could be established. It was found that the Helium - Neon laser did not produce sufficient energy to form good quality holograms, possibly due to excessive motion (eg. creep) of the specimens during the exposure times of the holograms. An Argon ion laser was substituted and high quality holograms were subsequently recorded. Exposure times with this laser were less than one second.

The initial double exposure holography tests showed that the number of fringes produced by deforming the specimen from 0 stress to just below failure was so great that the spacing between fringes were too fine to allow individual fringes to be visible. This was predicted by preliminary analysis using Young's Modulus and Poisson's Ratio for the materials and verified by initial holographic experimentation. To overcome this difficulty, an incremental double exposure approach was used. A series of double exposure holograms was recorded for increments in stress on the order of 3000 psi. The deformation corresponding to this applied stress caused a lesser number of fringes which were readily visible. The starting stress for one pair of holograms (at locations 1 and 2) was the final stress level for the previous pair. Incremental holograms were made in this manner from 0 stress until the specimen failed. The rate of application of stress between exposures of a single

hologram was on the order of 100 - 300 psi per second, followed by a period of no stress change of about two minutes during which time the hologram plates were exposed and replaced by the holograms used to record the next increment.

In this way, a successful series was run for one Jaspar Quartzite specimen and one Charcoal Granite specimen. Figures 11a and 11b show photographs of one representative holographic image for the lower (1) and upper (2) hologram positions from the Jaspar Quartzite series. Figures 12a and 12b show similar images from the Charcoal Granite series. These holograms, and the remaining holograms of both series are analyzed in detail in section 4.0.

3.2 Stored Beam (Motion Picture) Holography

It was desired that dynamic fringe patterns be recorded using high speed photography as the specimen was undergoing failure. To accomplish this, stored beam holography was employed. A Hycam 16 mm high speed motion picture camera was positioned at the lower (1) observer location.

To maximize the brightness of the specimens for the high speed photography, the lateral surfaces were coated with a pliable, thin film of diffusely reflecting white substance (a type of dye penetrant developer worked well). Figure 13 is a photograph of a coated Charcoal Granite cylinder.

The specimens were prestressed to a level (based on experience with previous specimens) not far from failure. A stored beam hologram was exposed, processed and repositioned in its holder (location 1). The specimen and hologram were illuminated by the laser light resulting in an interference pattern between the actual object and its holographic image.

a. Lower (O_1) View

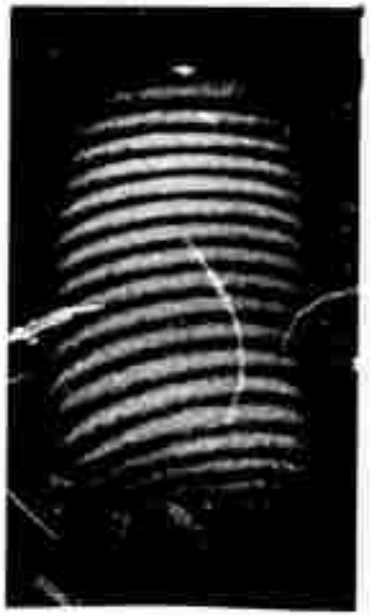

b. Upper (O_2) View

Figure 11: Photograph of the reconstructed double exposure images for one increment in stress (~3000 psi) of a Jaspar Quartzite specimen.

a. Lower (0_1) View

b. Upper (0_2) View

Figure 12: Photograph of the reconstructed double exposure image for one increment in stress (~3000 psi) of a Charcoal Granite specimen.

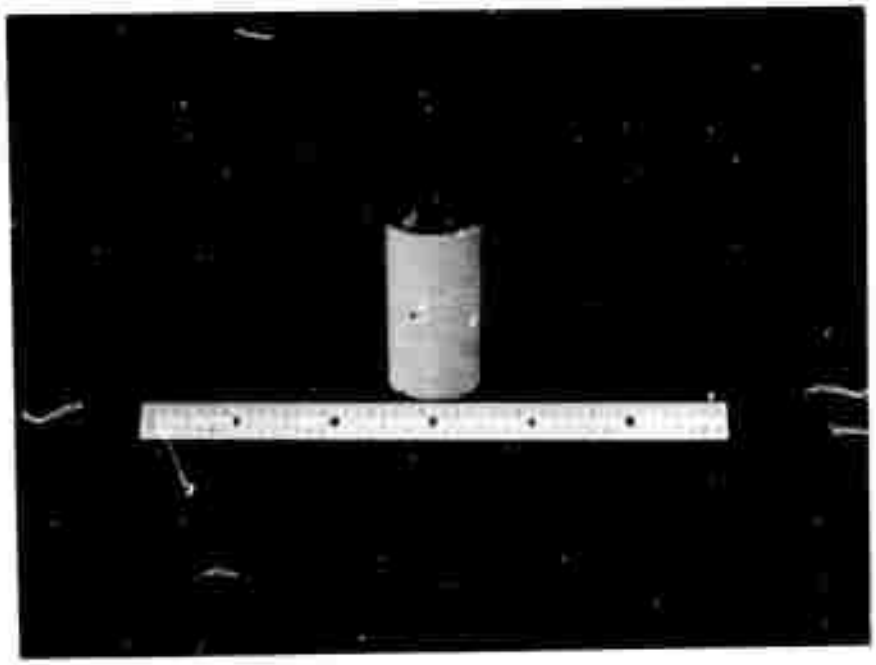

Figure 13: Photograph of a Charcoal Granite cylinder with whitened surface

The camera was started and then the stress increased until the specimen failed. The time required to reach failure was typically on the order of 3 to 10 seconds.

A number of problems developed with these experiments, limiting their success. One problem was creep of specimens under the applied prestress from the time the stored beam hologram made, processed and repositioned. When the stored beam hologram was replaced in the holder after processing, the deformation due to creeping led to a few (for the Jaspar Quartzite) to many (for the Charcoal Granite) fringes being present over the object. A second problem dealt with prestressing the specimens sufficiently close to failure. Statistical variations from sample to sample of the failure level and creep (some specimens broke at the constant prestress level while the stored beam hologram was being processed) prevented us from approaching too closely the failure level before stopping to record the stored beam hologram. Consequently, as the stress was further increased while the motion picture was recorded, the density of the fringe pattern became too great to be resolved even before the specimen failed.

However, meaningful motion pictures were obtained for one Jaspar Quartzite specimen and one Charcoal Granite specimen. Both records exhibited an initial fringe pattern (due to creep) at the beginning of the record. For both records, the fringe patterns became too dense to be resolved, considerably before failure occurred. Nevertheless, dynamically changing fringe patterns were recorded for both specimens in the early parts of the records. The Jaspar Quartzite record

was made at camera speed of 1500 frames per second. The Charcoal Granite record was made at a speed of 1000 frames per second. Both films have been sent to the Bureau of Mines.

Two techniques, which may overcome the difficulties mentioned above (either used together or separately) should be explored. First, to eliminate the problem associated with motion between the time the holographic exposure is made and the film developed and repositioned, the use of photochromics or thermoplastic recording methods are suggested. Photochromics and thermoplastics are materials which can be used to replate the function of the photographic film in the holographic process. Their main advantage is that their "development time" is on the order of milliseconds rather than 10-20 minutes, as in the case of photographic film. These materials and their applicability to holography are being explored by researchers; but are not yet used by the industry on a day-to-day basis in holography. Secondly, to eliminate the problem associated with capturing the fracturing event, a method of desensitized holographic interferometry should be explored. Here the illumination and viewing configurations in the holographic setup are arranged in such a manner that motion on the order of 200 microinches is required for a single fringe to form rather than motion on the order of 25 microinches as was the goal in this study. Several techniques are within the state-of-the-art but they require further development. Employing such techniques enable one to prestress the specimens to a level known to be below the fracture limit at the time the stored-beam hologram is

made. Then the specimen can be subjected to an additional load causing failure and the subsequent motion recorded via high-speed motion picture photography.

4.0 DATA REDUCTION

Since holographic interferometry is a measure of the entire displacement field, a large amount of data was generated in this program. It will be shown below that the two viewing-illumination configurations used were sufficient to determine the axial and radial displacement fields.

The basic method of data reduction relies on the interpretation given to the fringe patterns by Aleksandrov and Bronch-Bruevich (3) (described in Section 2.3.2 and briefly again below for the convenience of the reader). They show that the reconstructed image of a hologam exposed twice to a body which has been stressed between exposures will exhibit dark fringes on parts of the body wherever the condition

$$\vec{\delta}\cdot(\hat{s} + \hat{c}) = \frac{2n-1}{2}\lambda \qquad n = \pm1, \pm2, \pm3 \ldots \qquad (1)$$

is satisfied where

$\vec{\delta}$ = displacement vector

λ = wavelength of the light from the laser used to make and reconstruct the holographic images

$\hat{c}$ = unit vector in direction from object to illuminating source

$\hat{s}$ = unit vector in direction from the object through the hologram to the observer

The expression $\vec{\delta}\cdot(\hat{s} + \hat{c})$ is illustrated in Figure 14. The term $\hat{s} + \hat{c}$ represents a vector bisecting the angle between vectors $\hat{c}$ and $\hat{s}$, and having a length $2\cos((s,c)/2)$. Hence the expression $\vec{\delta}\cdot(\hat{s} + \hat{c})$ represents the component of deflection, δ_{cs}, in the direction of a unit vector bisecting the angle between the viewing and illuminating directions.

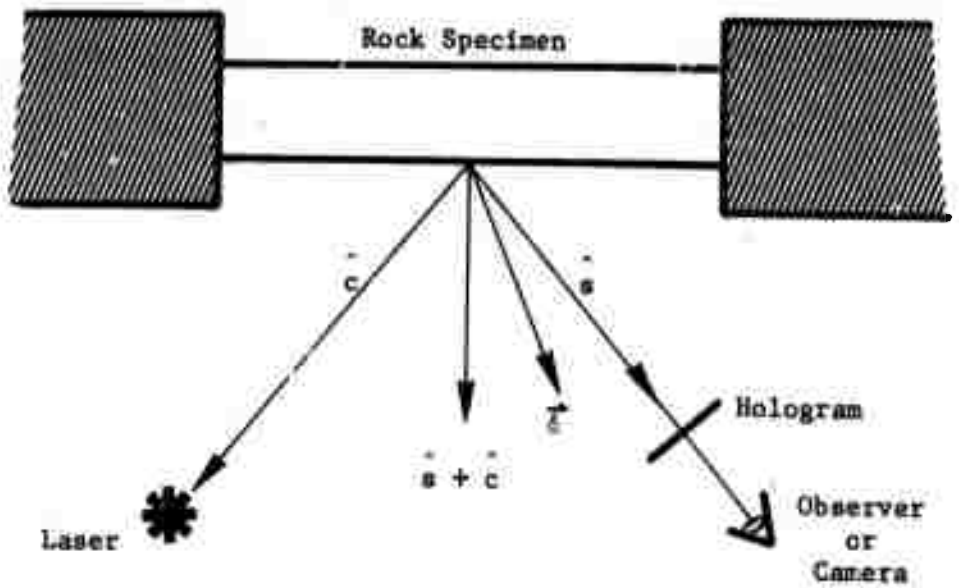

Figure 14: Vector diagram showing relations between illumination beam, hologram, and deformation vectors

A computer program, written using TRW Systems Group funds, was used to reduce the data contained on the holographic interferograms. A description of the code is given below. From the holograms made at two different illuminating-viewing configurations, the displacement field components

$$\begin{aligned} \delta^1(x_i) &\equiv \vec{\delta}(x_i)\cdot\left[\hat{s}^1(x_i) + \hat{c}^1(x_i)\right] = f(n_i,\lambda) \\ \delta^2(x_j) &\equiv \vec{\delta}(x_j)\cdot\left[\hat{s}^2(x_j) + \hat{c}^2(x_j)\right] = f(n_j,\lambda) \end{aligned} \tag{3}$$

are computed. The superscripts 1 and 2 denote the two different viewing-illumination configurations and the subscripts i and j denote arrays of position points and fringe order. Note that the displacement components need not be known at identical field points i.e., $x_i \neq x_j$. However, the displacement fields are smooth, and the discretely known fields can be

interpolated to give values at any point. Interpolating then we have the condition in Equation 3 that $x_i = x_j$ and therefore, the displacement components are known in <u>two directions</u> at <u>any point</u>. The radial and axial components of the displacement can be obtained from these known displacements as follows. By changing the coordinate systems from the base vectors $\hat{c}$ and $\hat{s}$ to base vectors in the direction of the radial and axial directions, the displacement vector can be written in terms of axial and radial components, viz

$$\vec{\delta} = \delta_a \hat{a} + \delta_r \hat{r}$$

where δ_a, $\hat{a}$ and δ_r, $\hat{r}$ are the axial component and associated unit vector and radial component and associated unit vector, respectively. Substituting Equation 2 in the system (1), we obtain the following system of equations

$$\begin{pmatrix} (\hat{s}^1 + \hat{c}^1)\cdot\hat{a} & (\hat{s}^1 + \hat{c}^1)\cdot\hat{r} \\ (\hat{s}^2 + \hat{c}^2)\cdot\hat{a} & (\hat{s}^2 + \hat{c}^2)\cdot\hat{r} \end{pmatrix} \begin{pmatrix} \delta_r \\ \delta_a \end{pmatrix} = \begin{pmatrix} \delta^1 \\ \delta^2 \end{pmatrix} \qquad (4)$$

The solution to these equations yield the axial and radial components of displacement at a desired point.

The programs used to solve these equations were written for use on the University of California at Santa Barbara (UCSB) On-Line Computer System. This system is part of the ARPA Computer Network. The program makes extensive use of graphic displays. TRW has applied the capabilities of remote on-line graphic consoles to a variety of engineering problems that are particularly amenable to solution by direct graphical interactive dialogue between the operator and the computer. The console configuration employed in the data reduction is shown in Figure 15. It consists of a dual keyboard to manipulate the computer software, a storage scope to

Figure 15: On-line computer system console used in the data reduction. Console consists of dual keyboard, storage scope and electronic input tablet (Grafacon).

view numerical and curvilinear data and an electronic input tablet (Grafacon) and stylus to enter graphical data directly. The tablet surface measures 10.24 inches square and provides a resolution of 100 points per inch. As a stylus comes in contact with the tablet surface, a small non-storable cursor appears on the scope providing convenient correspondence between the two devices, a particularly useful feature to detect from the tablet points portrayed on the scope. It was this last feature which greatly reduced the difficulty of the data reduction. Photographs of the reconstructed images of the holograms were placed on the tablet and the stylus was used to input the position of the fringes on the specimen. Once the fringe positions were inputed then the fringe order corresponding to each fringe was read in.

As an example of the data reduction procedure, one of the pairs of reconstructed images of the interferograms taken of Jaspar Quartzite will be examined in detail (Figure 11a and 11b). These interferograms are a measure of the incremental displacement induced due to an increment in load of 3,000 psi. These photographs were placed on the electronic tablet (Grafacon) and the stylus was placed on the fringes along the axis of the cylinder. This action caused the positions of the fringes to be entered into computer storage. The fringe order corresponding to each of these fringes were entered by the dual keyboard. The absolute fringe order was not known in these series of experiments. This introduces some ambiguity in the interpretations; however, other holographic methods such as finite fringe can be used in conjunction with the present technique to give the absolute order. For the sake of consistency in interpretation in these series of experiments, the fringe order was taken to be zero at one end of the specimen and the other fringe orders referenced to that fringe. The fringe orders for the pair were then interpolated to correspond to 21 evenly spaced positions along the specimen length. At each one of these positions the system of equations (Equations 4) were solved for the radial and axial displacements. Note that the viewing and illumination unit vectors vary in direction across the specimen and therefore the displacement sensitivity varies - an effect accounted for in the analysis. The incremental axial and radial displacements along the specimen for this incremental load are shown in Figures 16a and 16b.

Having computed all the incremental displacements in the manner described above, then the total displacements are just the sums of the

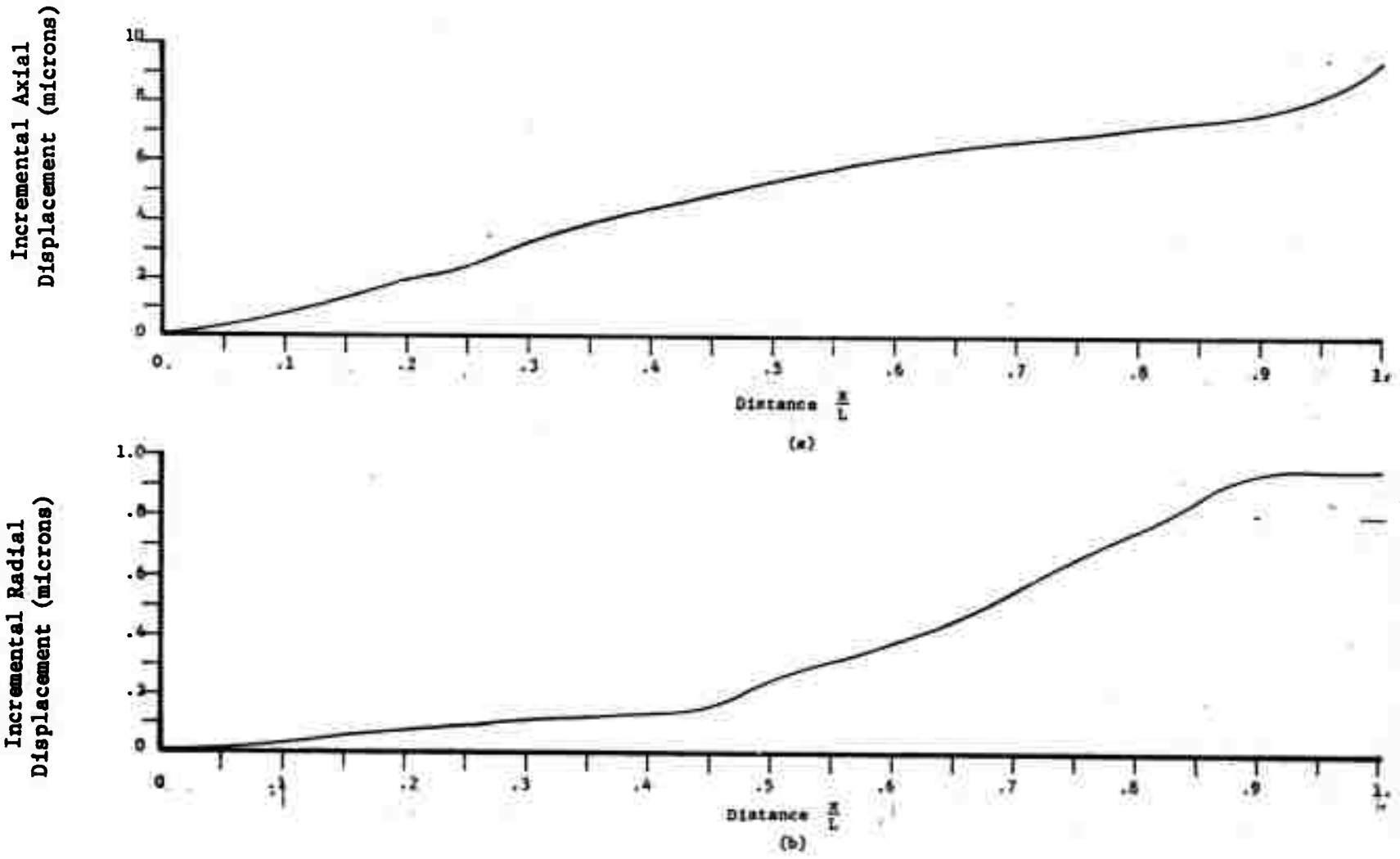

Figure 16: The incremental axial and radial displacement profiles at a loading level of 32,000 psi after an incremental load of ~ 3000 psi. The specimen was Jaspar Quartzite.

measured incremental displacements, i.e.,

$$U_z = \sum_i U_{zi} \tag{5}$$

$$U_r = \sum_i U_{ri} \tag{6}$$

where U_z and U_r represent the total axial and radial displacements, respectively. The axial strain, ε_z, is related kinematically to the axial displacements by

$$\varepsilon_z = \frac{\partial U_z}{\partial z} \tag{7}$$

The radial strain is only simply related to the radial surface displacements when the specimen is in a state of plane stress. When that is the case, the radial strain is given by

$$\varepsilon_r = \frac{U_r}{r} \tag{8}$$

Also, if the assumption of plane stress is valid then the Poisson ratio, ν, is given by

$$\nu = -\frac{\varepsilon_r}{\varepsilon_z} \tag{9}$$

In inhomogeneous materials such as rocks, strain fields induced by uniform external loads are locally spatially inhomogeneous. Holography measures the true surface displacement, which can be related to the local strain. One measure of the inhomogeniety of the axial strain field would be

$$\eta = \frac{|\varepsilon_z - \bar{\varepsilon}_z|}{\bar{\varepsilon}_z} \tag{10}$$

where $\bar{\varepsilon}_z$ is the local mean strain. The above number, $\eta \times 100$ would be the percentage deviation in the local strain field. The mean strain was calculated by using a first degree least-squares approximation.[4] For each position point, two points on either side of the position point were used in the smoothing. It was found that three iterations of the smoothing process was sufficient to suppress the local deviations and still retain the mean character of the function.

4.1 Jaspar Quartzite

A series of representative photographs of the reconstructed double exposure images for single increments in stress are shown in Figures 17a through 17p. A significant amount of information regarding the response of the Jaspar Quartzite specimen can be obtained by a visual examination of these photographs. The interferograms shown as lower views (1) were configured so that fringes would form only as a result of a radial motion; hence, the radial incremental displacement profiles closely follow the fringe position and number.

The interferograms shown as upper views (2) measured both radial and axial components of the displacements; however, since the axial displacements are greater than the radial, the fringes were formed primarily as a result of axial motion. The axial displacement is related to the number of fringes and the axial strain is proportional to the fringe spacings.

The series of photographs in Figures 17a through 17h are representative of the linear response regime (low stress). The radial and axial fringe patterns do not change significantly during loading in this regime. Examining the lower view in Figure 17e, the fringe spacing, and hence the radial displacement profile, increases from the top of the specimen to the bottom. In the corresponding upper view in Figure 17f the fringe spacing is approximately uniform, but with a greater fringe density near the ends. The finer fringe spacing indicates that the axial strains are larger in those regions.

a. Lower (1) view

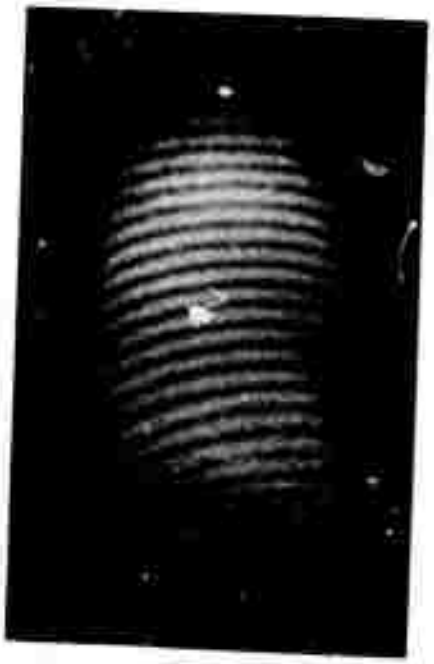

b. Upper (2) view

Total Stress = 12,700 psi

Figure 17: Photographs of the reconstructed double exposure images for one increment in stress (∿3000 psi) with a Jaspar Quartzite specimen

c. Lower (1) view

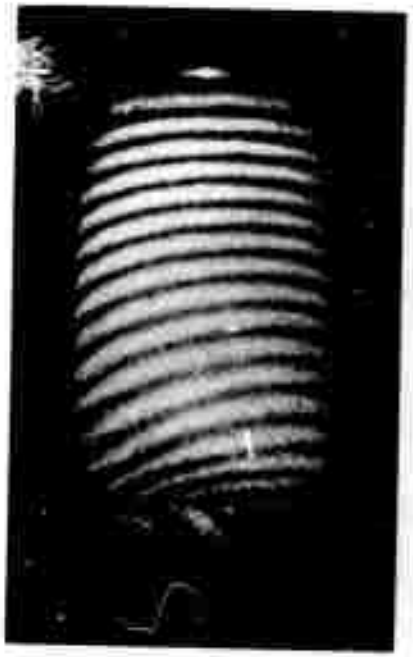

d. Upper (2) view

Total Stress = 23,900 psi

Figure 17: Photographs of the reconstructed double exposure images for one increment in stress (∿3000 psi) with a Jaspar Quartzite specimen

e. Lower (1) view

f. Upper (2) view

Total Stress = 33,700 psi

Figure 17: Photographs of the reconstructed double exposure images for one increment in stress (∿3000 psi) with a Jaspar Quartzite specimen

g. Lower (1) view

h. Upper (2) view

Total Stress = 38,000 psi

Figure 17: Photographs of the reconstructed double exposure images for one increment in stress (∿3000 psi) with a Jaspar Quartzite specimen

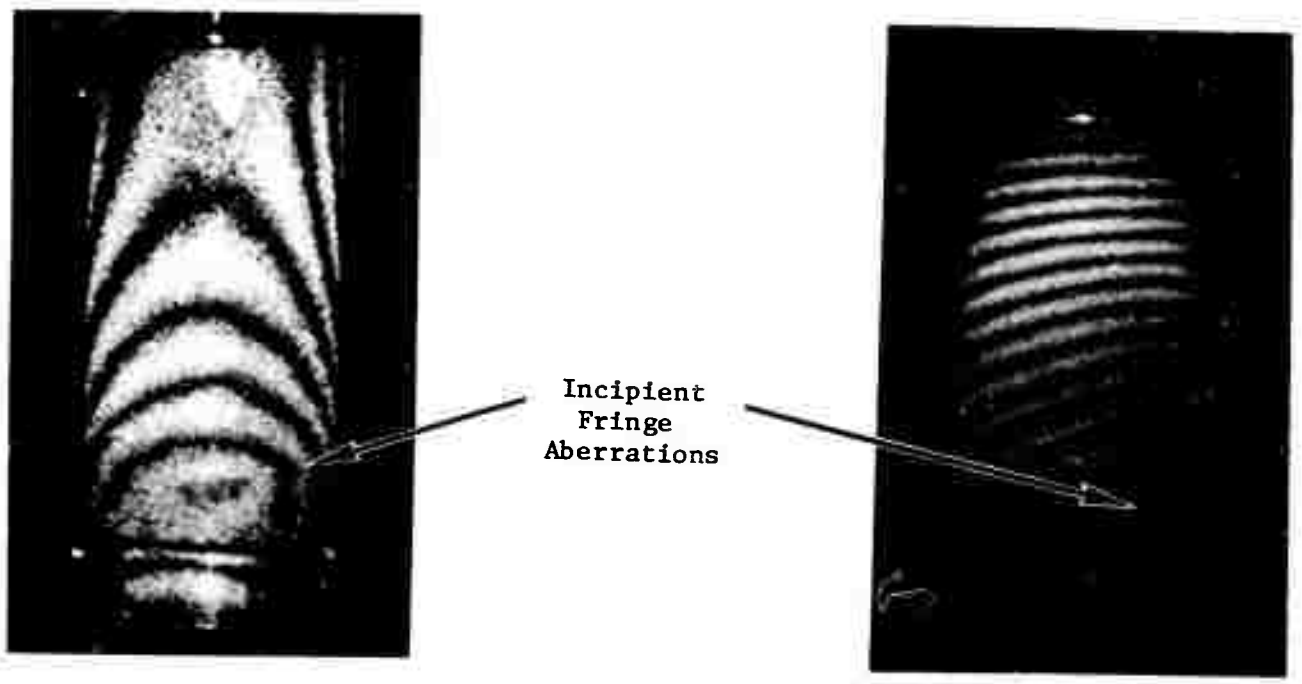

i. Lower (1) view

j. Upper (2) view

Total Stress = 46,400 psi

Figure 17: Photographs of the reconstructed double exposure images for one increment in stress (~3000 psi) with a Jaspar Quartzite specimen

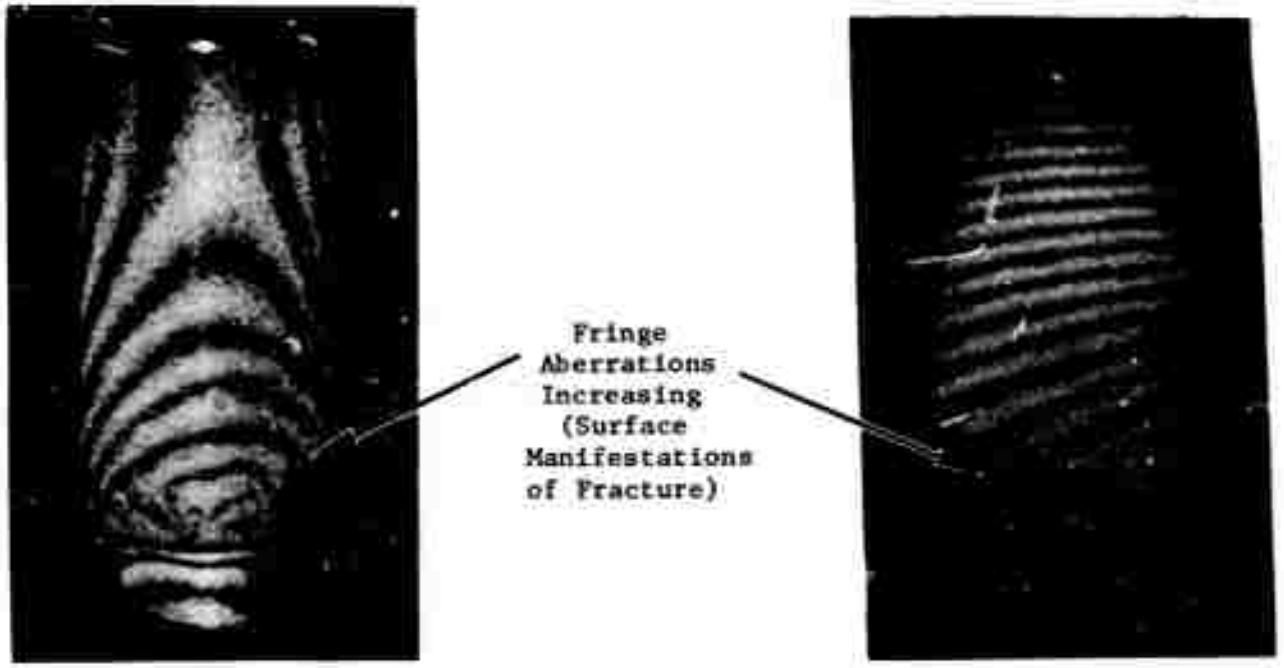

k. Lower (1) view

1. Upper (2) view

Total Stress = 57,600 psi

Figure 17: Photographs of the reconstructed double exposure images for one increment in stress (~3000 psi) with a Jaspar Quartzite specimen

m. Lower (1) view

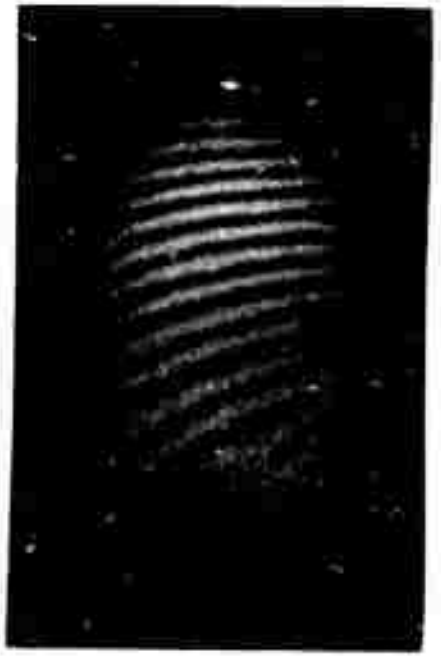

n. Upper (2) view

Total Stress = 63,200 psi

Figure 17: Photographs of the reconstructed double exposure images for one increment in stress (∿3000 psi) with a Jaspar Quartzite specimen

o. Lower (1) view

p. Upper (2) view

Total Stress = 65,400 psi

Figure 17: Photographs of the reconstructed double exposure images for one increment in stress (∿3000 psi) with a Jaspar Quartzite specimen This was the last stress increment before failure.

The series of photographs in Figures 17i through 17p are representative of the nonlinear response regime. This regime occurs for this specimen and loading configuration at a load of 46,400 psi. In this regime there are fringes which are discontinuous or have discontinuities in their derivatives as depicted in Figures 17i through 17ℓ. It is thought that these discontinuities are surface manifestations of fracturing of the specimen. As the stress level is increased until failure. the discontinuities grow and increase in spatial frequency.

The above qualitative interpretation of the fringe patterns has been borne out by detailed calculations. The calculations using the previously discussed numerical techniques were carried out for all of the incremental loadings. These results are given below. The total axial and radial displacement profiles are shown in Figures 18 and 19, respectively, for the loading of 21,200 psi; 43,600 psi; and 65,400 psi. The latter stress level corresponds to the stress just before failure.

An overall view of the response of cylinders can be obtained from Figures 20 and 21. These are three dimensional graphics, with the distance axis representing the equally spaced stations on the specimen at which the calculations were performed - the stress axis representing the total axial stress applied to the specimen and the z axis representing the total axial and radial displacements, respectively. Note in these figures that the axial and radial displacements are larger near one end of the specimen than the other. It is in this region that fracturing first occurred.

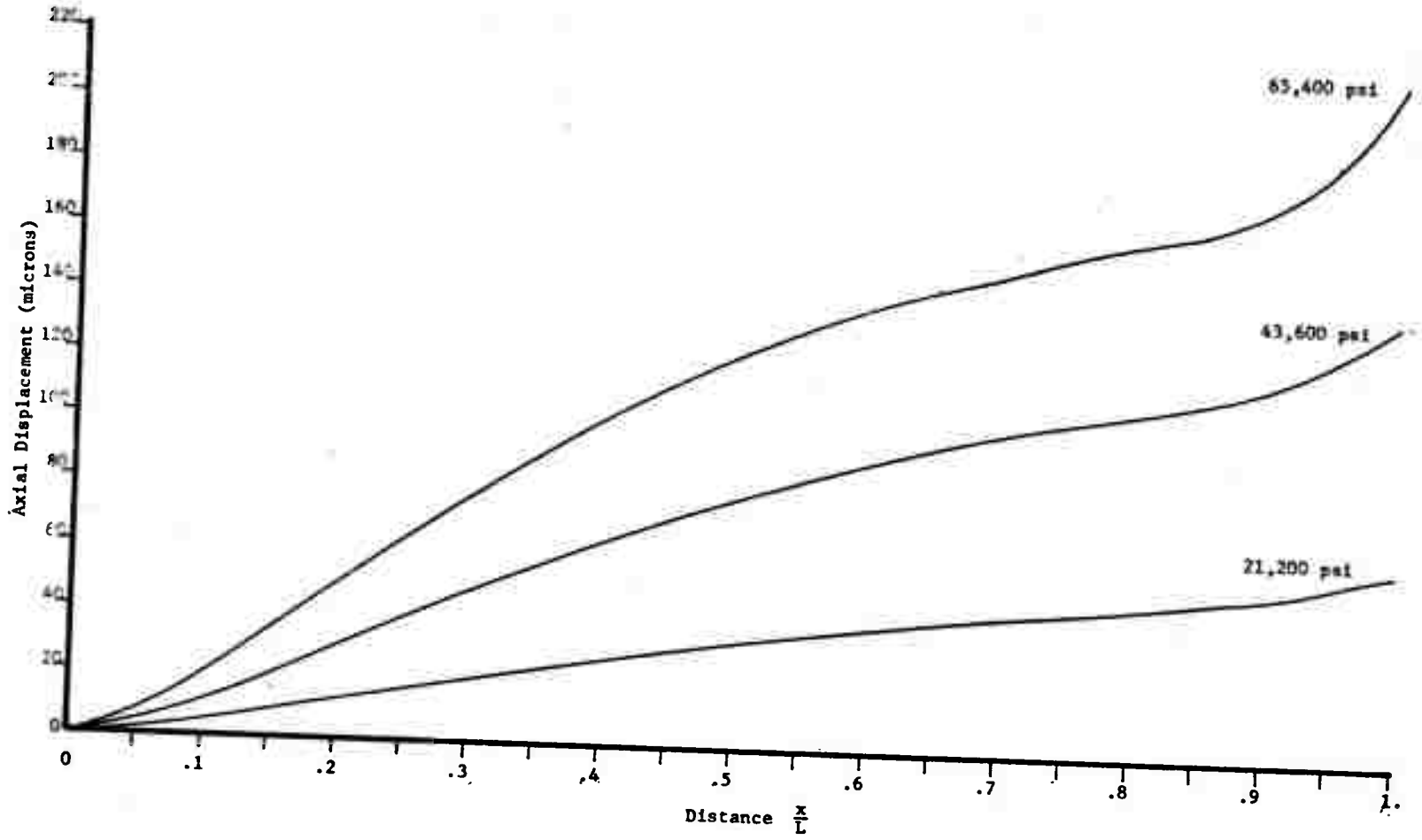

Figure 18: The axial displacement profiles in Jaspar Quartzite for various loading levels

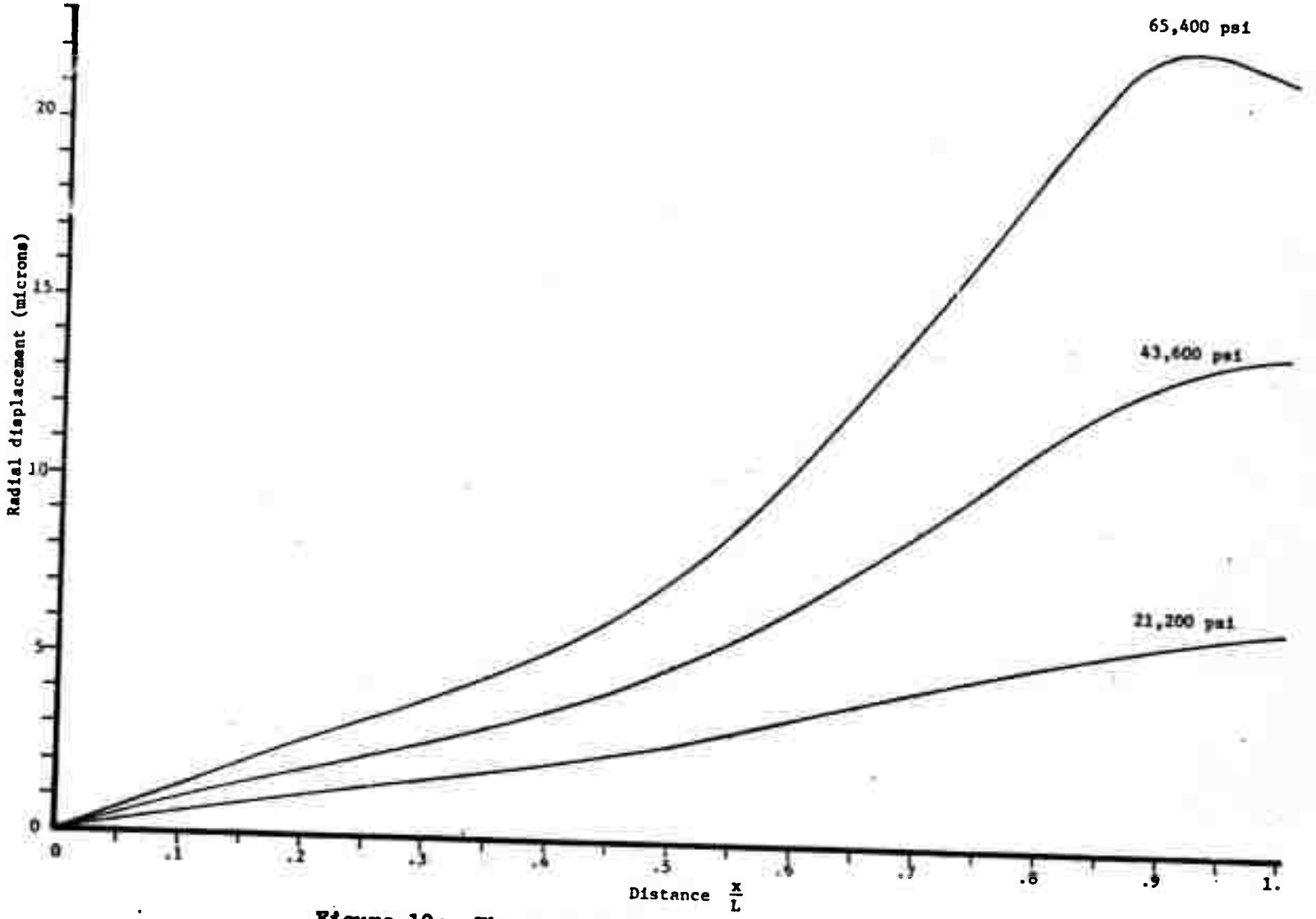

Figure 19: The radial displacement in Jaspar Quartzite for various loading levels

Figure 20: The total axial displacement profiles in the Jaspar Quartzite specimen as a function of load up to failure.

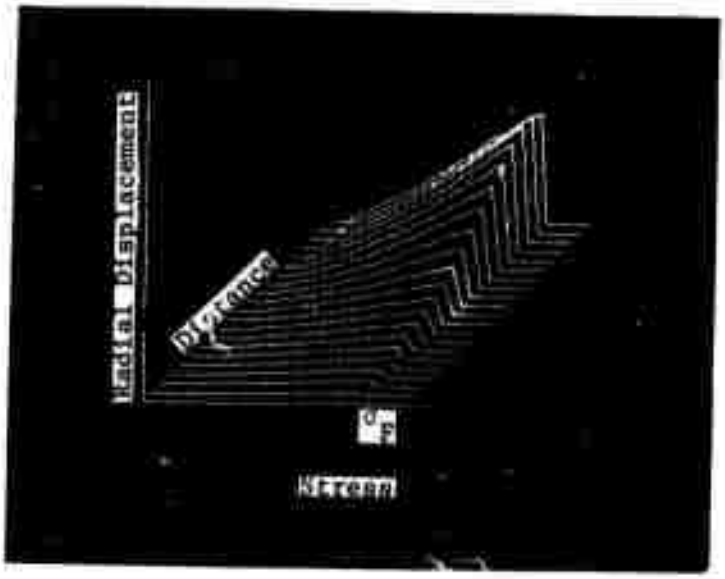

Figure 21: The total radial displacement profiles in the Jaspar Quartzite specimen as a function of load up to failure.

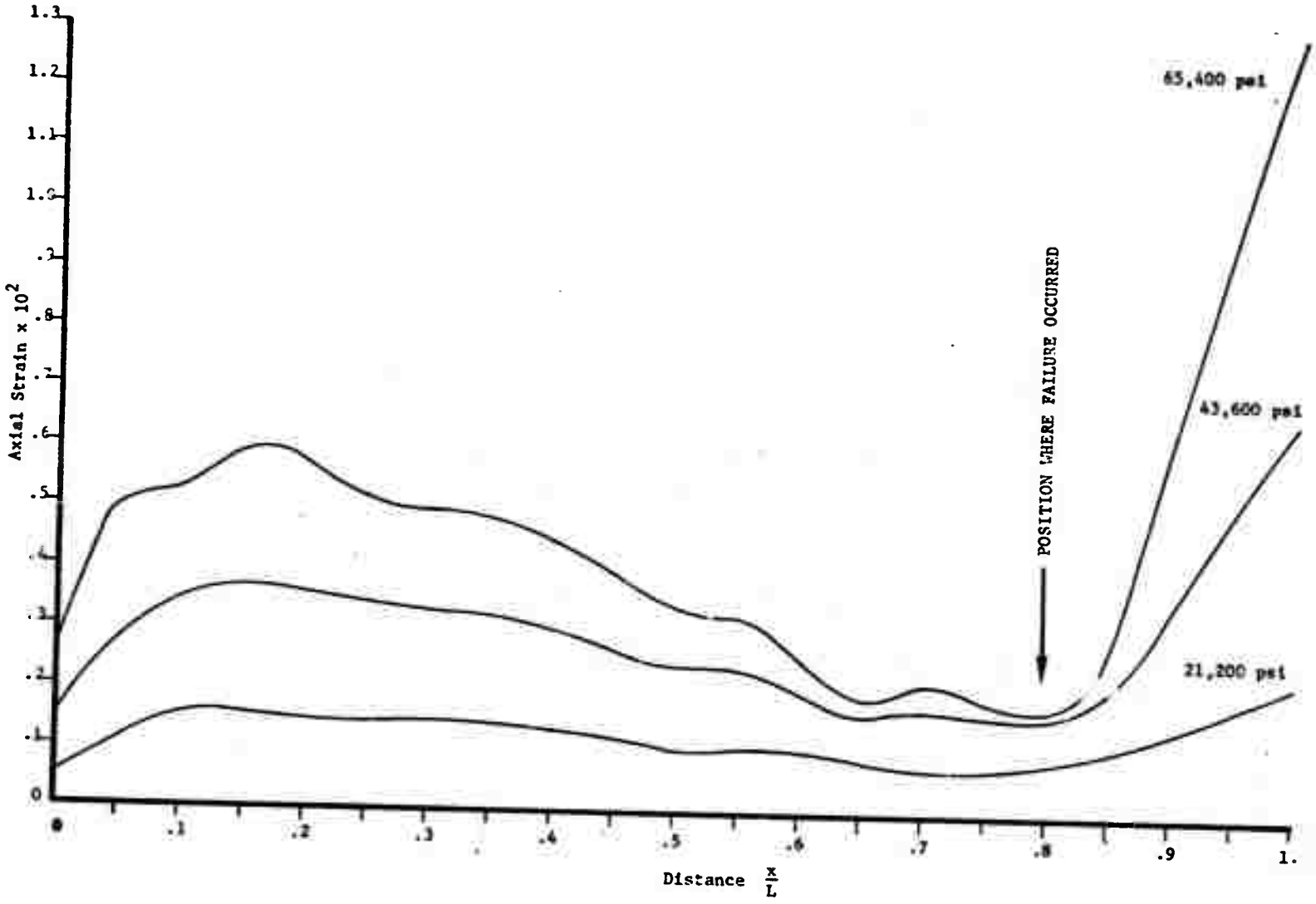

Figure 22: The axial strain profiles in Jaspar Quartzite for various loading levels.

The axial strain was calculated from the axial displacements and the profiles at three stress levels are presented in Figure 22. The profile histories are shown in Figure 23. The axial strain appears to be a sensitive measure of the nonlinear response of this specimen. The axial strains are very large in the regions where the specimen fractured, i.e., for positions greater than x/L = .8 in Figure 22.

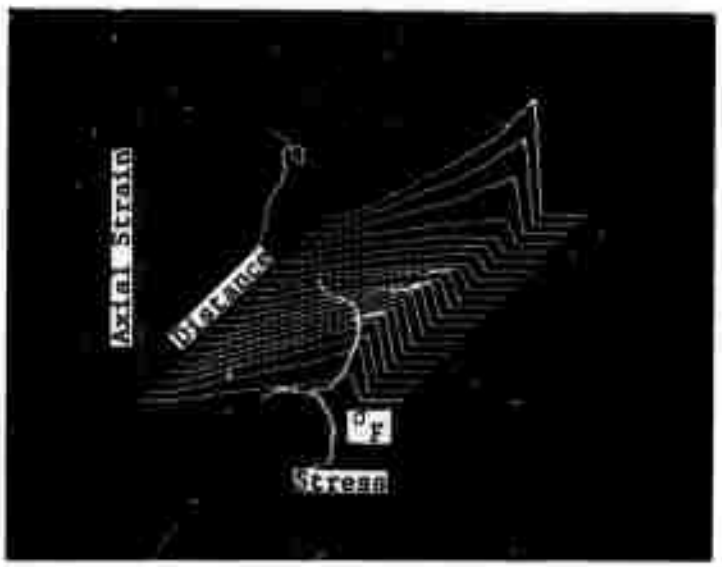

Figure 23: The axial strain profiles in the Jaspar Quartzite specimen as a function of load up to failure.

The above results on Jaspar quartzite demonstrate that double exposure holography can be used to measure the entire induced displacement field. The photographs of fringe patterns enable one to quickly assess the degree of local homogenity in the displacement fields and determine regions of strain concentration. It was also demonstrated that the photographs of the holograms can be interpreted to give quantitiative data. The current drawbacks to the technique are that many exposures have to be obtained when the total displacements are large. Also, refinements are needed in order to determine the absolute fringe order.

4.2 Charcoal Granite

A representative series of photographs of the results of the experiments on Charcoal Granite is presented in Figures 24a through 24p. One apparent difference between the fringe patterns for the Jaspar Quartzite and the Charcoal Granite is in the nonuniformity of the Charcoal Granite fringes. Furthermore because Poisson's ratio is larger for Charcoal Granite, the lower views (corresponding to radial deflections) have a greater number of fringes as compared to Jaspar Quartzite for an equal number of fringes on the upper view. The Charcoal Granite specimens responded in an approximately linear manner, without large scale discontinuities in fringe patterns up to a load of approximately 35,000 psi. (See Figures 24a through 24j.) Examining the lower views in this series and remembering that they are representative of the incremental radial displacement profiles, it can be seen that when the specimen was initially loaded that the specimen had a maximum radial displacement at the bottom. However, referring to Figure 24a, as the load was increased to 9,800 psi the maximum position had shifted to the top and remained in that position until failure.

As the loading was increased, the global nonuniformities in the fringes grew larger. At approximately 39,400 psi, there appear large scale deviations in the fringe patterns. See Figures 24m and 24n. This is the beginning of the nonlinear regime and extends until the specimen fails. Again, these large scale fringe deviations are thought to be the result of local fracturing of the specimen. See Figures 24m through 24p. The fringe order in the fractured region is sometimes difficult to

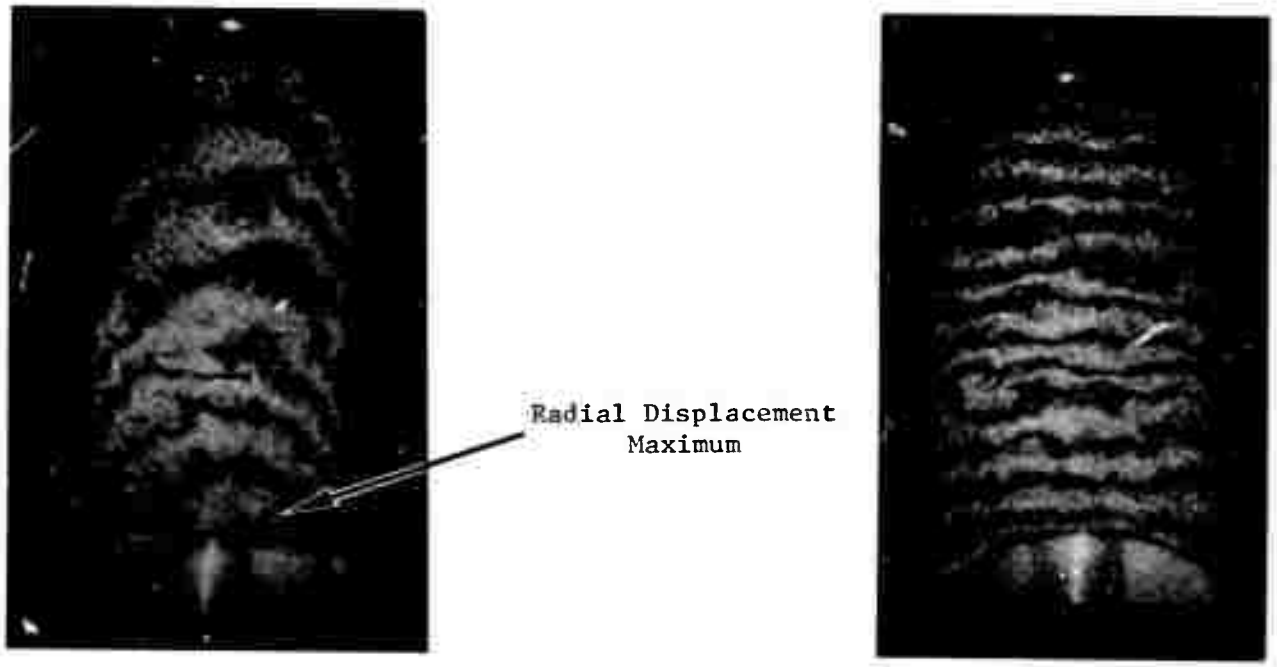

a. Lower (1) view

b. Upper (2) view

Total Stress = 4,200 psi

Figure 24: Photographs of the reconstructed double exposure images for one increment in stress (~3000 psi) with a Charcoal Granite specimen

c. Lower (1) view

d. Upper (2) view

Total Stress = 7,000 psi

Figure 24: Photographs of the reconstructed double exposure images for one increment in stress (∿3000 psi) with a Charcoal Granite specimen

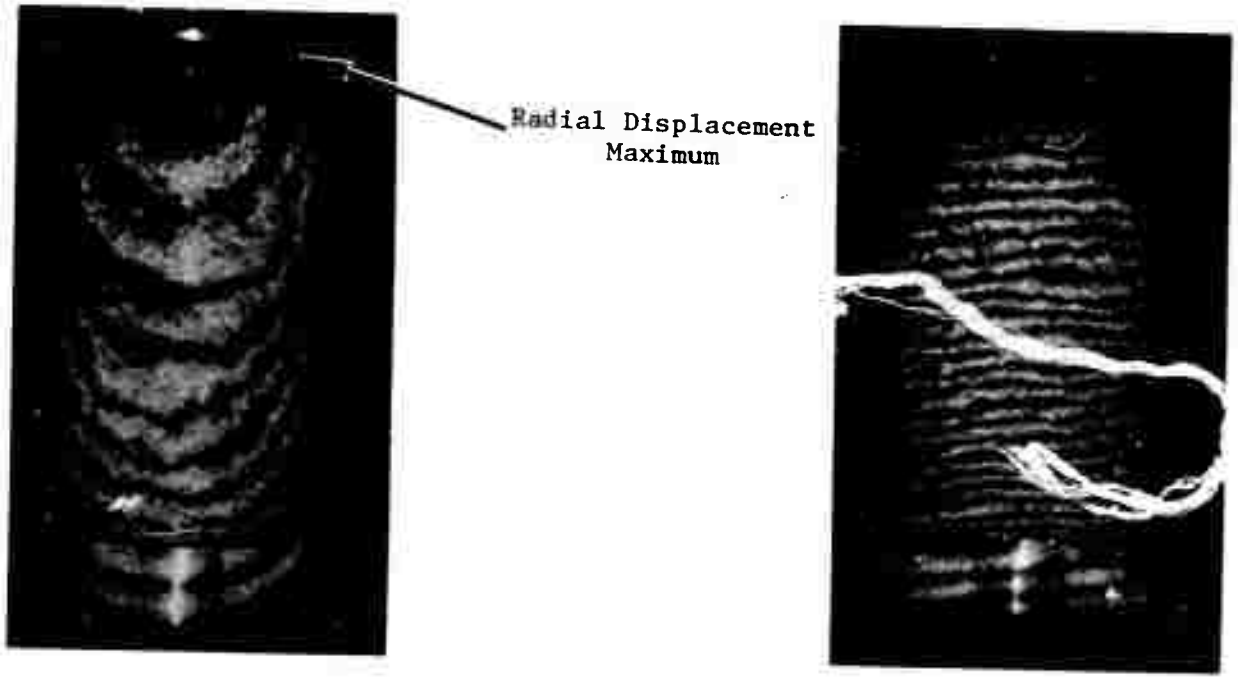

e. Lower (1) view

f. Upper (2) view

Total Stress = 9,800 psi

Figure 24: Photographs of the reconstructed double exposure images for one increment in stress (∿3000 psi) with a Charcoal Granite specimen

g. Lower (1) view

h. Upper (2) view

Total Stress = 23,900 psi

Figure 24: Photographs of the reconstructed double exposure images for one increment in stress (~3000 psi) with a Charcoal Granite specimen

i. Lower (1) view

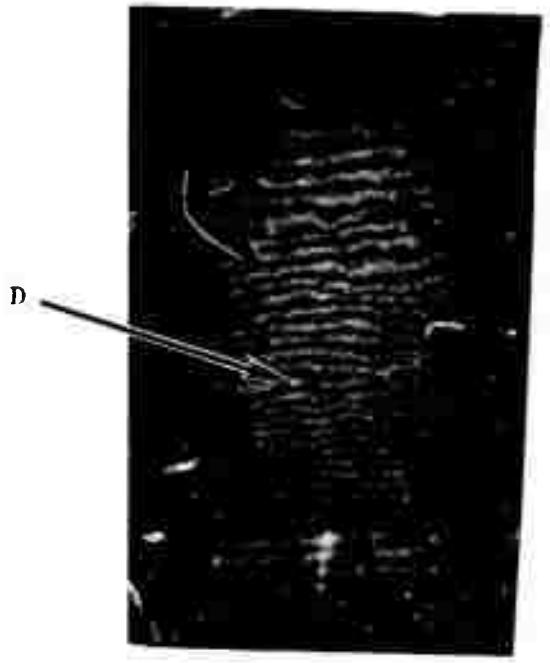

j. Upper (2) view

Total Stress = 32,300 psi

Figure 24: Photographs of the reconstructed double exposure images for one increment in stress (∿3000 psi) with a Charcoal Granite specimen

k. Lower (1) view

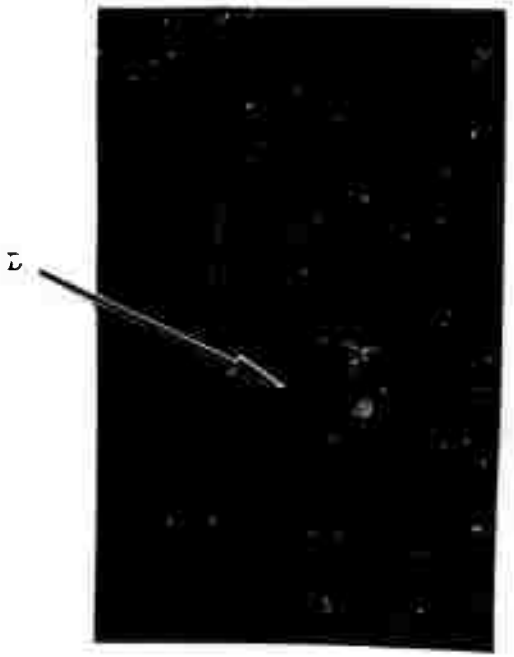

1. Upper (2) view

Total Stress = 35,100 psi

Figure 24: Photographs of the reconstructed double exposure images for one increment in stress (~3000 psi) with a Charcoal Granite specimen

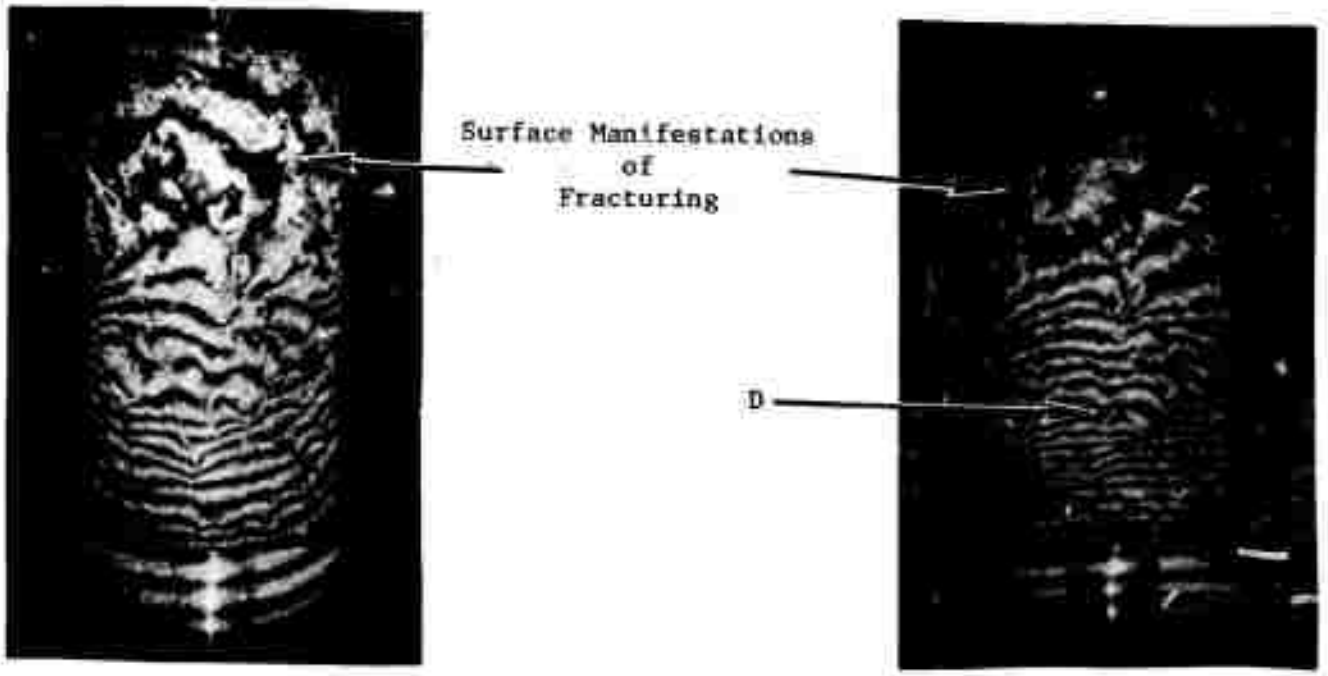

m. Lower (1) view

n. Upper (2) view

Total Stress = 39,400 psi

Figure 24: Photographs of the reconstructed double exposure images for one increment in stress (∿3000 psi) with a Charcoal Granite specimen

o. Lower (1) view

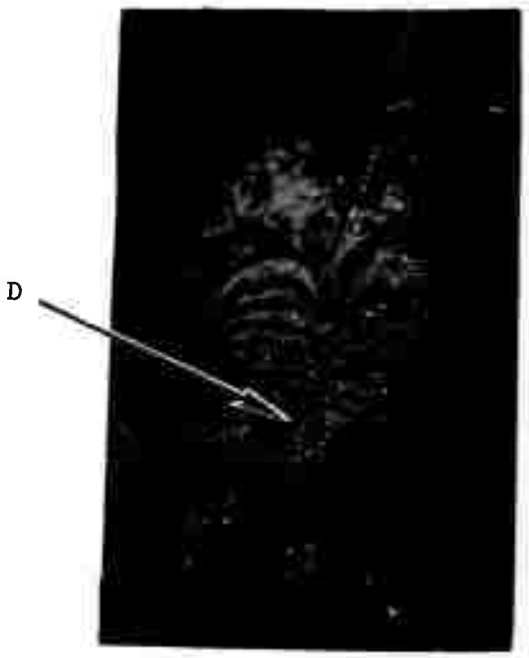

p. Upper (2) view

Total Stress = 40,700 psi

Figure 24: Photographs of the reconstructed double exposure images for one increment in stress (~3000 psi) with a Charcoal Granite specimen

to determine; however, this region is spatially rather uniform, i.e., exhibiting a low radial fringe density. Hence, the errors introduced by estimating fringe order should be small.

Numerical calculations were performed for all of the incremental loadings. The total axial and radial displacement profiles for the loading levels of 12,600; 29,500; and 40,800 psi are shown in Figures 25 and 26. This latter stress level corresponds to the stress just before failure. The axial and radial displacement profile histories, as a function of load up to failure, are given in Figures 27 and 28. The total axial and radial response for this loading configuration was globally more homogeneous than the Jaspar Quartzite even though locally the Charcoal Granite is more inhomogeneous. The axial strain was calculated from the axial displacements. The strain profiles at three stress levels, including the increment just before failure, are given in Figure 29. Two additional views of the axial profile histories as a function of load are presented in Figures 30a and 30b. These figures illustrate that the mean axial strain was fairly uniform across the specimen even though the local fluctuations were relatively large. Note in Figure 30b the growth of axial strain deviations at various positions along the specimen as the load is increased. For example, the deviations at the position D in Figure 30b correspond to the fringe deviations indicated by a local inhomogeniety at the point D indicated in Figures 24j, 24l, 24n, and 24p. The mean strain, $\bar{\varepsilon}_z$, was calculated as described in Section 4.0 and parameter $|\varepsilon_z - \bar{\varepsilon}_z|/\bar{\varepsilon}_z$ was computed as a function of load. See Figure 31. This parameter is a measure of the absolute deviation of the strain from the local mean. It is interesting that this measure is not a sensitive

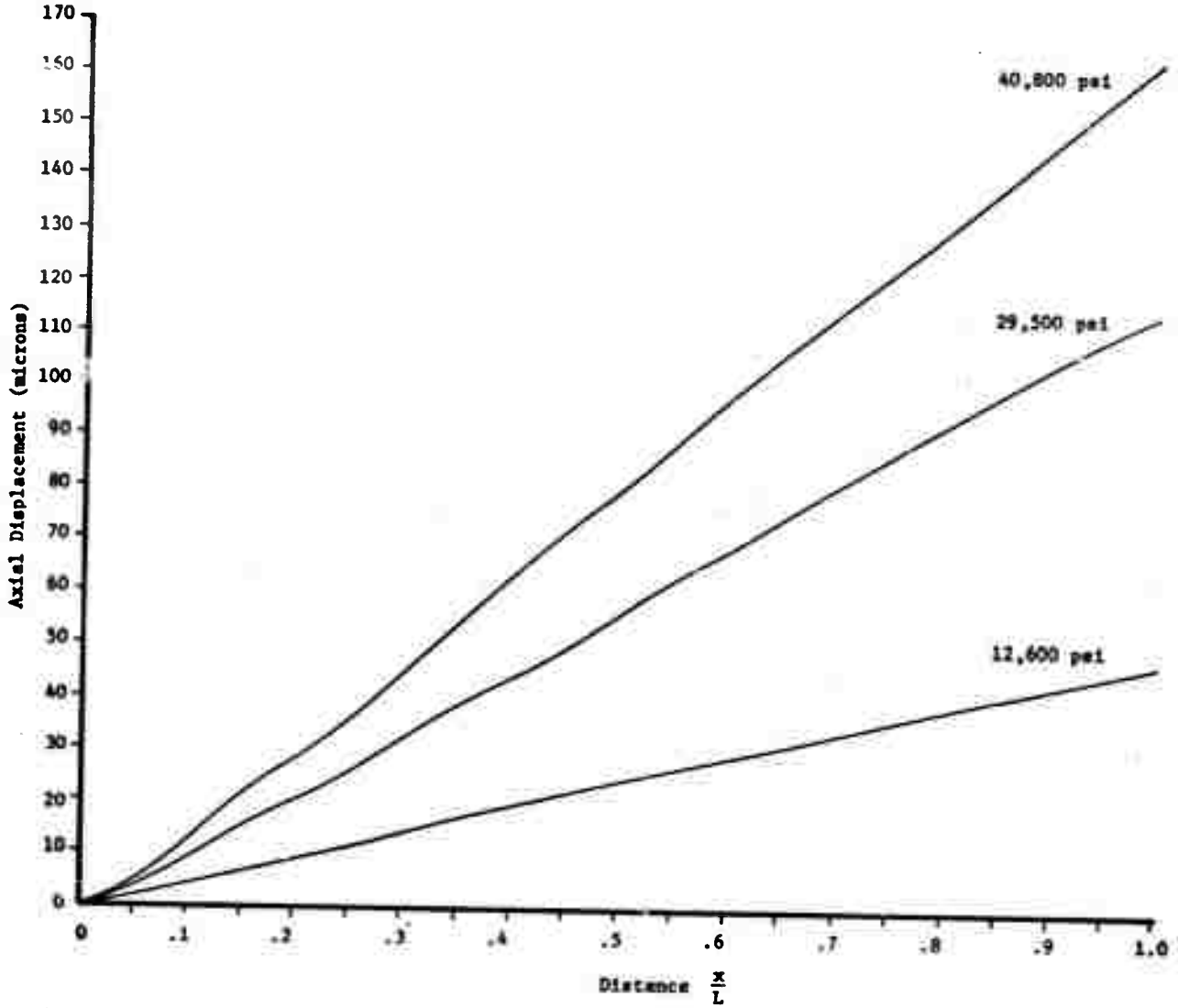

Figure 23: The axial displacement profiles in Charcoal Granite at various loading levels.

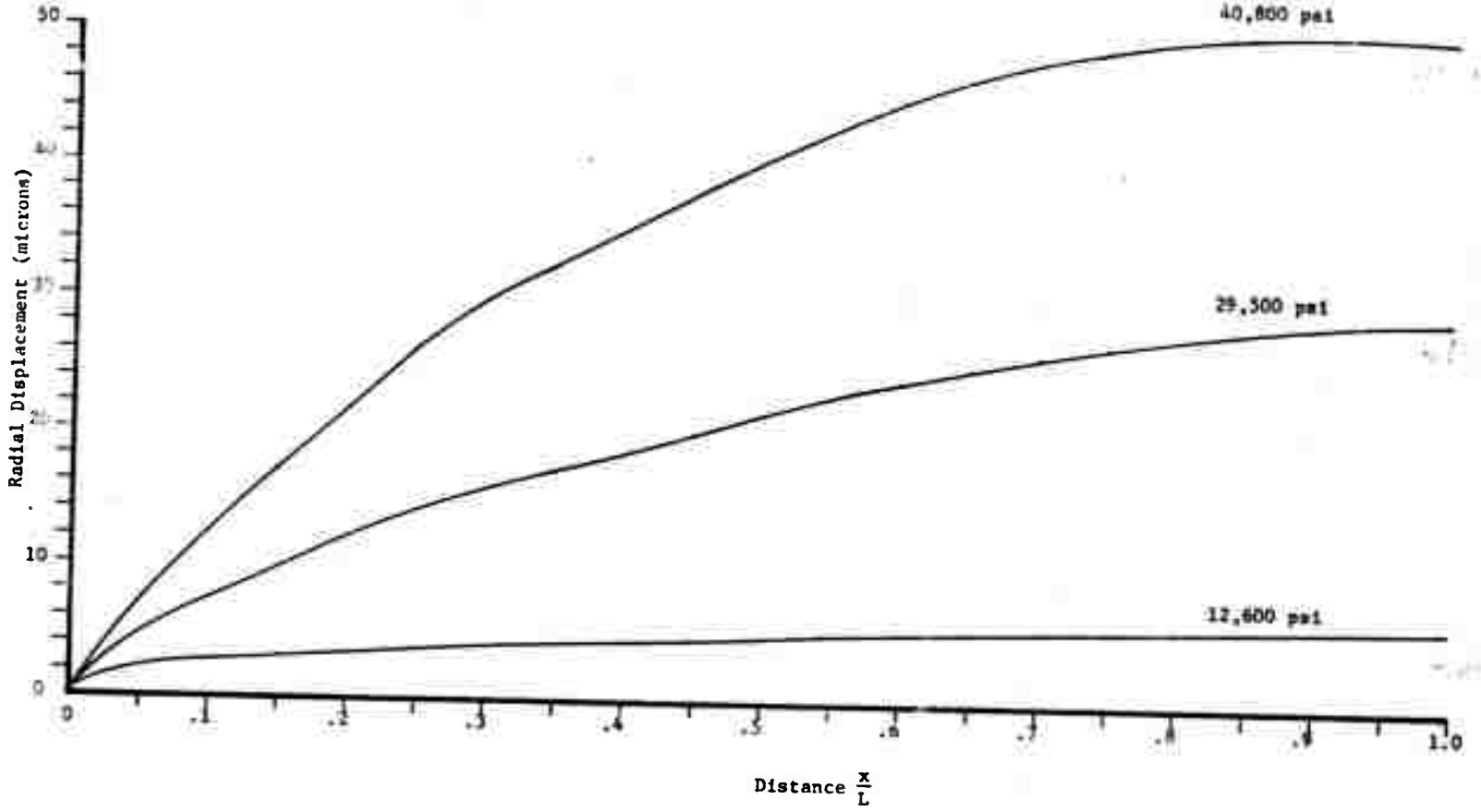

Figure 26: The radial displacement profiles in Charcoal Granite at various loading levels.

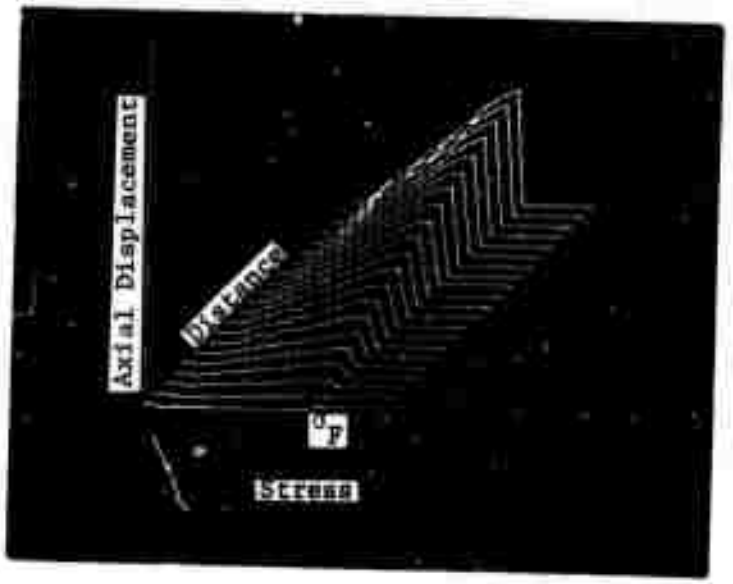

Figure 27: The total axial displacement profiles in Charcoal Granite as a function of load up to failure.

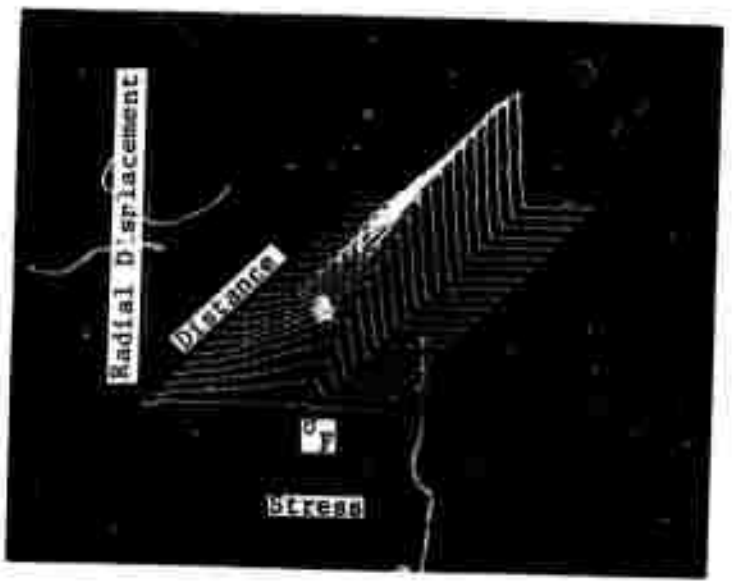

Figure 28: The total radial displacement profiles in Charcoal Granite as a function of load up to failure.

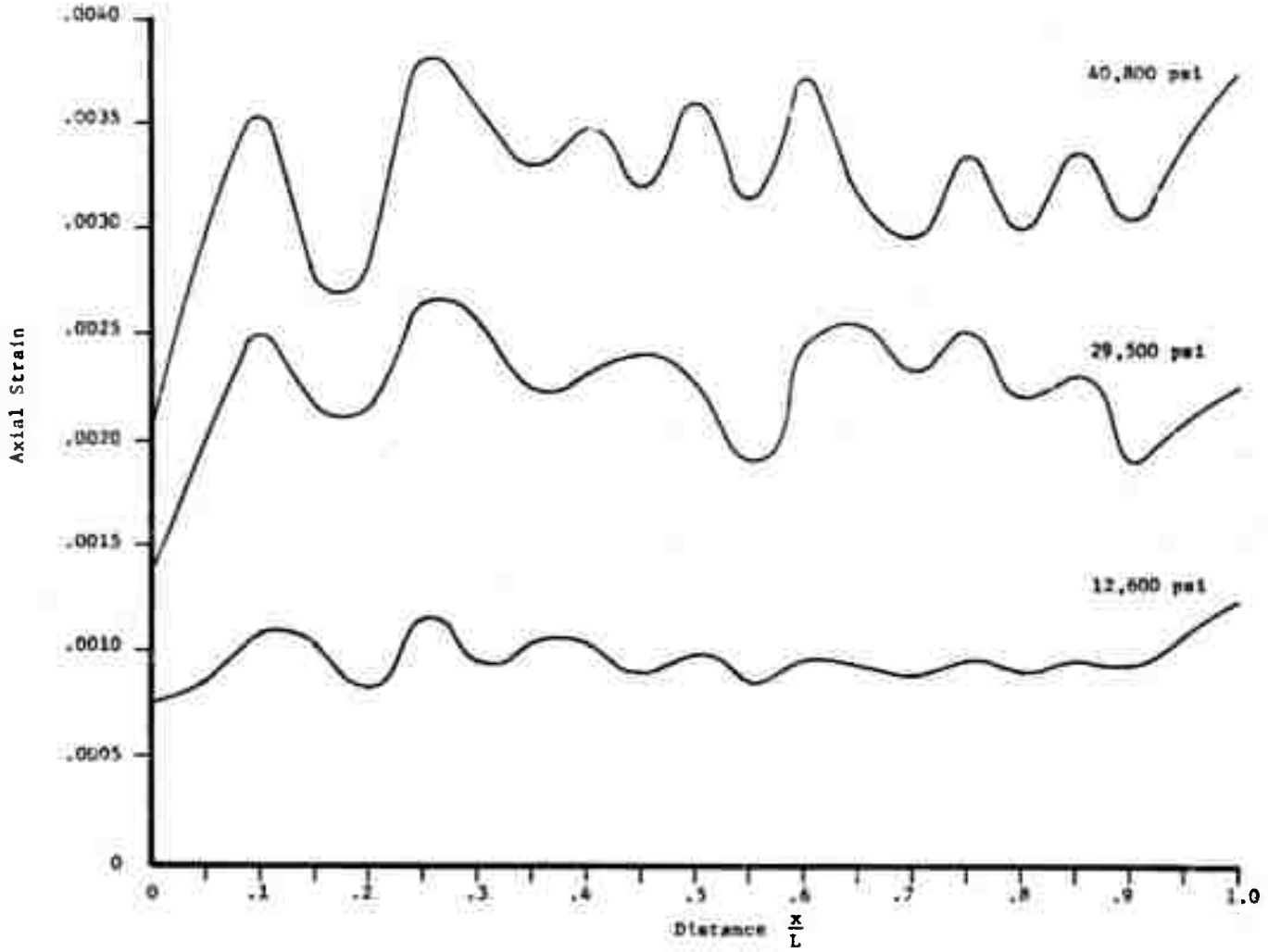

Figure 29 : The axial strain profiles in Charcoal Granite for various loading levels.

function of the load, i.e., percentage increase in the local strain inhomogeniety does not change dramatically for a given position. For this test configuration the maximum value of the deviation was $\approx .2$ and the spatial average, i.e., the average strain deviation across the specimen length was $\approx .08$.

If the assumption of plane stress is made then the radial strain can be readily calculated. However, the radial displacement profile indicates that the specimen was not strictly in a state of plane stress. With this reservation, the radial strain is given in Figure 32.

The above results confirm that double-exposure holography can be used to measure the entire displacement field. The fringe patterns dramatically reveal the inhomogeneity of the local displacement fields. These local inhomogeneities have been for the first time quantified, thus demonstrating a strong point of the holographic technique, the extreme sensitivity. Again, the difficulty with the technique is that many exposures have to be obtained when the total displacements are large. This problem can be circumvented to a degree by desensitizing. The sensitivity can be decreased by approximately an order of magnitude by various configurations of the viewing and illumination angles. Also, it was previously mentioned that the absolute fringe order is not known unambiguously. By using finite fringe interferometry and possibly simultaneously double exposure interferometry, the absolute order can be determined. However, the implementation of these techniques was out of the scope of this present effort.

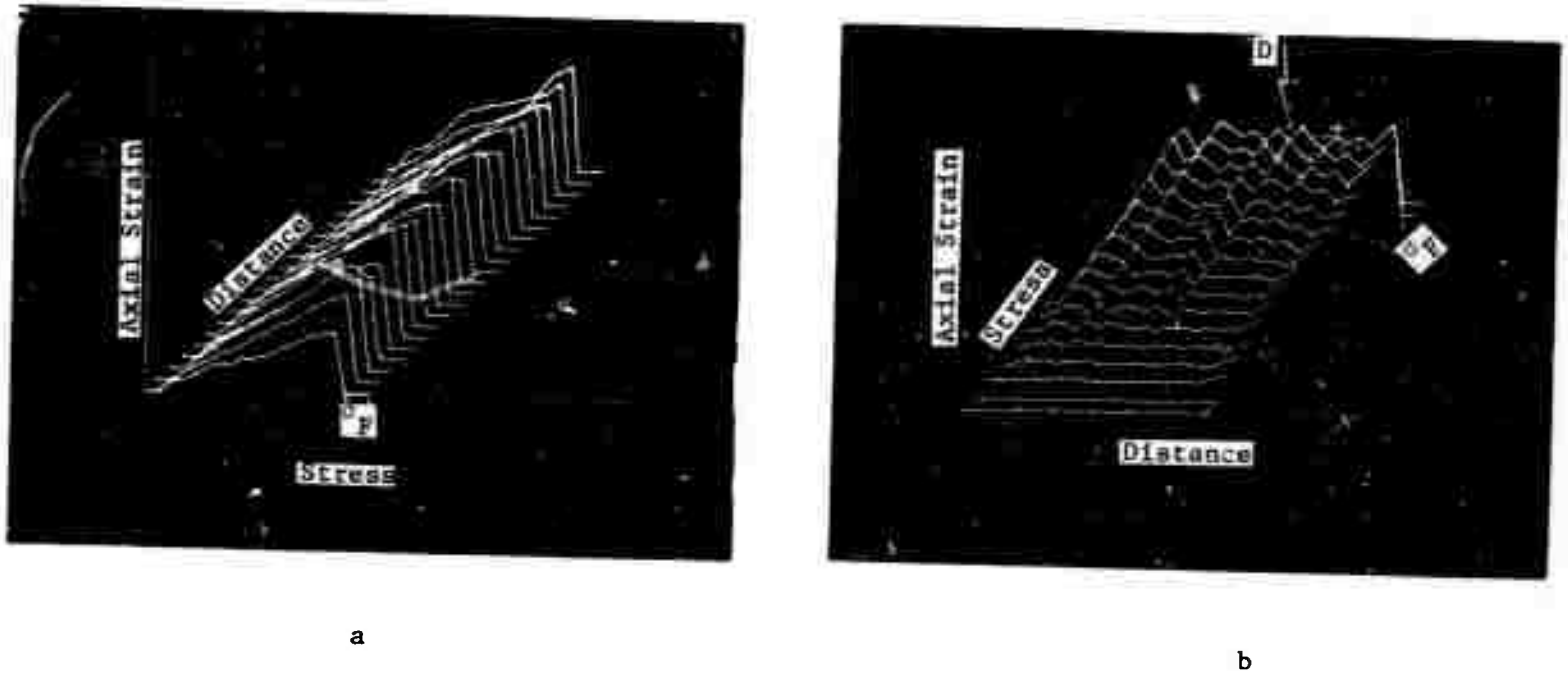

a

b

Figure 30: Two views of the axial strain profiles in Charcoal Granite as a function of load up to failure.

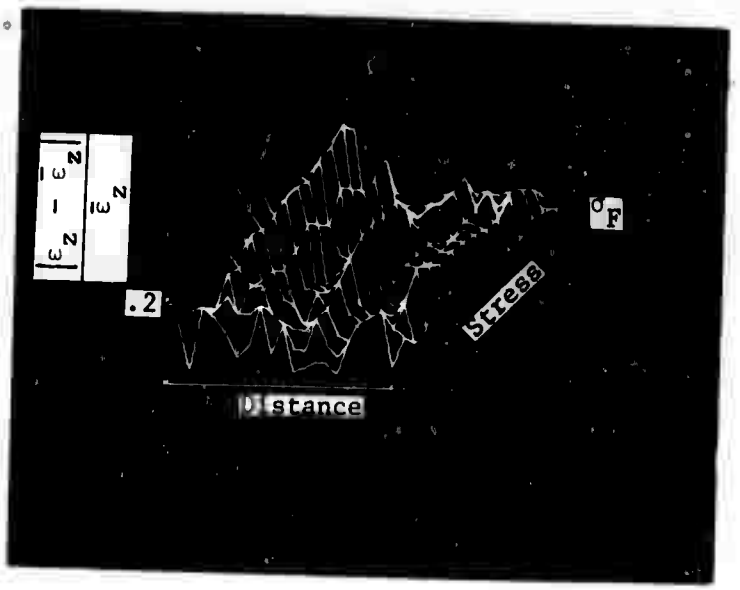

Figure 31: The relative axial strain deviation in the Charcoal Granite specimen as a function of load up to failure.

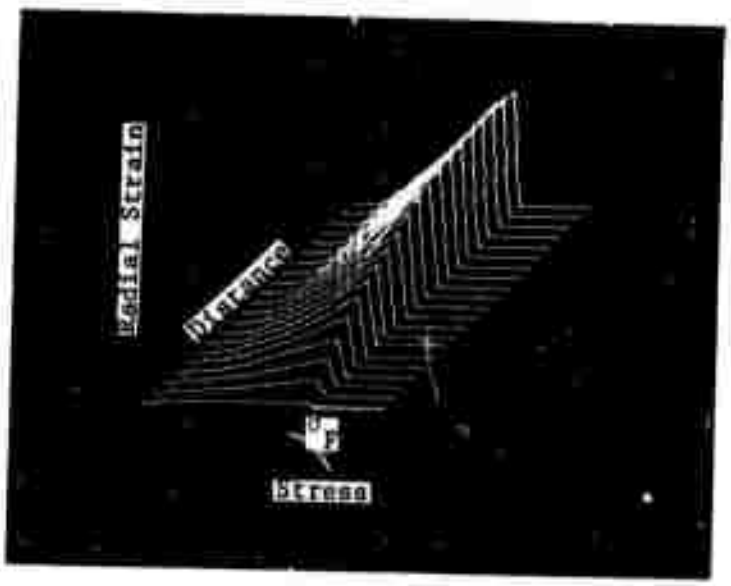

Figure 32: Radial strain profiles in Charcoal Granite as a function of load up to failure. A state of plane stress was assumed for these calculations.

5.0 REFERENCES

1. Gabor, D., "Microscopy by Reconstructed Wavefronts," Proc. Roy. Soc., Series A, Vol. 197, 1949.

2. Lieth, E. N., and Upatnieks, J., "Wavefront Reconstruction with Diffuse Illumination and 3-Dimensional Objects," J. Opt. Soc. Am., Vol. 54, November 1964.

3. Aleksandrov, E. B., and Bonch-Bruevich, A. M., "Investigation of Surface Strains by the Holographic Techniques," Soviet Physics, Technical Physics, Vol. 12, No. 2, August 1967, p. 258ff.

4. Schreiner, R. N., private communication.